



Western Michigan University  
ScholarWorks at WMU

---

Master's Theses

Graduate College

---

12-2005

## Ductile Regime Nano-Machining of Silicon Carbide

Biswarup Bhattacharya

Follow this and additional works at: [https://scholarworks.wmich.edu/masters\\_theses](https://scholarworks.wmich.edu/masters_theses)



Part of the Mechanical Engineering Commons

---

### Recommended Citation

Bhattacharya, Biswarup, "Ductile Regime Nano-Machining of Silicon Carbide" (2005). *Master's Theses*. 4837.

[https://scholarworks.wmich.edu/masters\\_theses/4837](https://scholarworks.wmich.edu/masters_theses/4837)

This Masters Thesis-Open Access is brought to you for free and open access by the Graduate College at ScholarWorks at WMU. It has been accepted for inclusion in Master's Theses by an authorized administrator of ScholarWorks at WMU. For more information, please contact [wmu-scholarworks@wmich.edu](mailto:wmu-scholarworks@wmich.edu).



# DUCTILE REGIME NANO-MACHINING OF SILICON CARBIDE

by

Biswarup Bhattacharya

A Thesis  
Submitted to the  
Faculty of The Graduate College  
in partial fulfillment of the  
requirements for the  
Degree of Master of Science in Engineering (Mechanical)  
Department of Mechanical and Aeronautical Engineering

Western Michigan University  
Kalamazoo, Michigan  
December 2005

Copyright by  
Biswarup Bhattacharya  
2005

## ACKNOWLEDGMENTS

This work would not have been possible without the advice and support of many people. First, and foremost, I would like to thank my advisor Dr. John Patten for providing me the opportunity and guidance throughout this project. Great thanks go to Dr. Philip Guichelaar for his immense support and providing space in his laboratory to set up my experiments, and also training me to use the white light interference microscope. I would like to thank Dr. Pnina Ari-Gur for training me to use the scanning electron microscope. I would like to acknowledge the collaborative work with the High Temperature Materials Laboratory (HTML) located at Oak Ridge National Laboratory. Many thanks go to Dr. Peter Blau for providing me with the opportunity to work at HTML. Many thanks to Jason Braden and Dr. Jane Howe for helping me with my experiments at HTML. Special thanks to Dr. Rob Eversole for his support in imaging some of my tools. Special thanks go to Dr. Muralidhar Ghantasala, Dr. Philip Guichelaar and Dr. Pnina Ari-Gur, for serving on my thesis committee and providing advice and review of the thesis. Great thanks to Jerry Jacob, Roshan Joseph and Ramesh Chandra for working with me on various experiments in this study. I would also like to thank the Department of Mechanical Engineering at the Western Michigan University for giving me the opportunity to study in their graduate program.

## Acknowledgements — Continued

Finally, I would like to express my acknowledgements to Third Wave Systems and the National Science Foundation for having funded this work.

Biswarup Bhattacharya

## DUCTILE REGIME NANO-MACHINING OF SILICON CARBIDE

Biswarup Bhattacharya, M.S.E.

Western Michigan University, 2005

This thesis describes experimental work carried out to study the ability to ductile single point diamond turn both polycrystal Silicon Carbide (SiC) and chemically vapor deposited (CVD) SiC. A Precitech diamond turning machine was used for ductile regime machining of polycrystal SiC at depths of 10 and 25 nm. The possibility of machining SiC in the ductile mode was substantiated by post process analysis of the chips collected during machining and the surface profiles. The force data obtained during machining was recorded and compared later with the different depth of cuts. An investigation into the ability to single point diamond turn (SPDT) CVD SiC with single crystal diamond tool was performed. Initial scratching experiments were performed to determine the ductile to brittle transition (DBT) depth for CVD SiC. Two different vendors of CVD SiC were used for the experiments (Poco Graphite Inc and Coors Tek Inc). The DBT depths for the Poco Graphite Inc. was found to be 550 nm and for the Coors Tek Inc 400 nm. Scratching experiments confirmed the existence of ductile mode in these materials which lead to SPDT experiments of CVD SiC to achieve surface roughness of less than 20 nm. These later tests were performed at actual depths of 200-300 nm and feed of a 1  $\mu\text{m}/\text{rev}$ .

## TABLE OF CONTENTS

ACKNOWLEDGEMENTS.....	ii
LIST OF TABLES.....	ix
LIST OF FIGURES.....	x
1. INTRODUCTION.....	1
1.1. Silicon Carbide.....	2
1.2. Polycrystalline Silicon Carbide.....	4
1.3. CVD Coated Silicon Carbide.....	5
1.4. Conventional Manufacturing.....	6
1.5. Precision Machining.....	7
1.6. Project Goals.....	8
2. BACKGROUND OF RESEARCH.....	10
2.1. Origin of Ductility.....	10
2.2. Phase Transformation.....	12
2.3. Material Removal /Chip Formation.....	13
2.4. Surface Characteristics.....	16
2.5. Effect of Rake Angle and Cutting Edge Radius of the Tool.....	17
2.6. Tool Wear.....	18
2.7. Machining Forces.....	20

## Table of Contents — Continued

3. DUCTILE REGIME NANO-MACHINING OF POLYCRYSTALLINE SILICON CARBIDE .....	22
3.1. Introduction.....	22
3.2. Experimental Setup for Machining of Polycrystalline SiC.....	23
3.3. Results.....	24
3.3.1. Force Plots of Cutting and Thrust Forces ..... for Different Cutting Tools	24
3.3.2. Surface Roughness.....	27
3.3.3. Tool Wear.....	29
3.3.4. Post Experimental Analysis.....	30
3.4. Discussion.....	32
3.4.1. Forces and Coefficient of Friction.....	32
3.4.2. Thermal Effects.....	33
3.5. Conclusion.....	33
4. DETERMINATION OF DUCTILE TO BRITTLE TRANSITION DEPTH (DBT) FOR CVD COATED SILICON CARBIDE .....	35
4.1. Introduction.....	35
4.2. Pre-experimentation Process.....	36
4.3. Scratching using a 5 $\mu$ m Diamond Stylus Tip.....	37
4.4. Results from Scratching with 5 $\mu$ m Diamond Stylus.....	37
4.4.1. Coors Tek Sample.....	37
4.4.2. Poco Graphite Sample.....	38



## Table of Contents — Continued

### CHAPTER

4.5. Inclined Plate Experiment.....	40
4.6. Results from Inclined Plate Experiment.....	42
4.7. Scratching of using a 12.5 $\mu\text{m}$ Diamond Stylus.....	43
4.7.1. Coors Tek Sample.....	43
4.7.2. Poco Graphite Sample.....	44
4.8. Results from Scratching using 12.5 $\mu\text{m}$ Diamond Stylus.....	44
4.8.1. Coors Tek Sample.....	44
4.8.2. Poco Graphite Sample.....	47
4.9. Coefficient of Friction.....	51
4.10. Tool Degradation.....	52
4.11. Discussion.....	54
4.12. Conclusion.....	54
5. SINGLE POINT DIAMOND TURNING (SPDT) OF.....	55
CHEMICALLY VAPOR DEPOSITED (CVD) COATED SILICON CARBIDE (SiC)	
5.1. Introduction.....	55
5.2. Polishing of CVD SiC.....	56
5.3 Machining Parameters. ....	56
5.4. Experimental Setup for SPDT of CVD SiC .....	57
5.5. Results.....	58

## Table of Contents — Continued

### CHAPTER

5.5.1. Machining Time.....	58
5.5.2. Surface Roughness.....	58
5.5.3. Tool Wear.....	61
5.5.4. Depth of Cut.....	61
5.5.5. Feed/ Rev.....	63
5.5.6. Material Removal.....	63
5.6. Discussion.....	64
5.7. Conclusion.....	64
5.8. Ongoing Work on SPDT of CVD SiC.....	64
6. DETERMINATION OF A DUCTILE RESPONSE AND A.....	66
DUCTILE TO BRITTLE TRANSITION DEPTH OF QUARTZ (Infrasil 302)	
6.1. Introduction.....	66
6.2. Scratching of Quartz with 5 $\mu$ m Diamond Stylus .....	67
6.3. Inclined Plate Experiment.....	68
6.3.1. Experimental Setup for Inclined Plate Experiment.....	69
6.3.2. Results from Inclined Plate Experiment.....	70
6.4. Discussion.....	72
6.5. Conclusion.....	72

## Table of Contents — Continued

7. CONCLUSION.....	73
7.1. Concluding Remarks.....	73
7.1.1. Polycrystalline SiC.....	73
7.1.2. CVD SiC.....	73
7.1.3. Quartz.....	74
7.2. Future Developments.....	74
7.2.1. Polycrystalline SiC.....	74
7.2.2. CVD SiC.....	74
7.2.3. Quartz.....	75
REFERENCES.....	76
APPENDICES.....	79
A. Material Properties of Polycrystalline SiC, CVD SiC and Quartz.....	79
B. Ductile to Brittle Transition Depth Calculations.....	80
C. Calculations for Required Load for SPDT of SiC.....	81
D. Calculations for Volume of Material Removal after SPDT of CVD SiC.....	83
E. Calculation for Validation of Scratching Experiments.....	85
F. Diamond Cutting Tool Design used for Different Experiments.....	86

## LIST OF TABLES

4.1. Surface roughness details of CVD coated SiC samples.....	36
5.1. Comparison of programmed and achieved depth of cuts.....	61
6.1. Summary of experiments performed to determine DBT in quartz .....	72

## LIST OF FIGURES

1.1: Flow chart for production of polycrystalline SiC by firing of consolidated powders .....	4
2.1: Chip profile geometry for single point machining using a round nose cutting tool .....	14
2.2: Stress Field generated in a chip .....	14
2.3: Model of micro-fracture damage transitions in ductile regime machining.....	15
2.4: Schematic model showing wear of the tool .....	18
2.5: Flank wear vs machining time .....	19
2.6: Schematic of orthogonal cutting model showing the direction of forces .....	20
3.1: Experimental setup for machining of polycrystalline SiC.....	23
3.2: CAD drawing showing the specifications of the SiC tube .....	23
3.3: Comparison of forces for different depths of cut (Chardon tool).....	25
3.4: Comparison of force ratio for 10 and 25 nm depth of cuts.....	25
3.5: Comparison chart for forces achieved from Chardon and Edge tools at 10nm depth of cuts .....	26
3.6: Force ratio for Chardon and Edge tool at 10 nm depths of cut.....	26
3.7: Surface profiles for the SiC tube after machining .....	27
3.8: Surface roughness plot for 10 nm depth of cut showing the best surface roughness achieved .....	28
3.9: Surface roughness plot for 25 nm depth of cut showing the best surface roughness achieved .....	28

## List of Figures — Continued

3.10: Optical microscope image of tool wear, the tool is at 45 deg to the microscope's lens, looking perpendicular to the rake face .....	29
3.11: Schematic representation of tool wear .....	30
3.12: Image of diffraction pattern showing the halo ring for amorphous nature of the material .....	31
3.13: TEM image of a ductile chip from machining SiC .....	31
3.14: TEM EDS analysis of the ductile chip .....	32
4.1: Wyko image of completely ductile scratch for Coors Tek sample using 5 $\mu$ m diamond stylus .....	38
4.2: Force plot for the scratch made on Coors Tek material using 5 $\mu$ m diamond stylus .....	38
4.3: Wyko image showing DBT depth behind the tool for Poco Graphite sample using 5 $\mu$ m diamond stylus .....	39
4.4: Force and acoustic emission (AE) data for Poco Graphite sample .....	40
4.5: Experimental setup for inclined plate experiment .....	41
4.6: Schematic representation of the inclined plane experiment geometry .....	42
4.7: Wyko image of the DBT depth for Poco Graphite material using flat nose diamond tool .....	43
4.8: Force plot for center of scratch showing DBT for Poco Graphite material using a flat nose diamond tool .....	43
4.9: Wyko image showing the initial part of scratch for Coors Tek sample using 12.5 $\mu$ m stylus .....	45
4.10: Force and acoustic emission (AE) plot for initial part of the scratch for Coors Tek sample using 12.5 $\mu$ m stylus .....	45

## List of Figures — Continued

4.11: Wyko image of the DBT depth for Coors Tek sample using 12.5 $\mu$ m stylus .....	46
4.12: Force profile for DBT depth of Coors Tek sample using 12.5 $\mu$ m stylus .....	46
4.13: Wyko image showing the brittle fracture region after DBT depth for Coors Tek sample using 12.5 $\mu$ m stylus .....	47
4.14: Wyko image of the starting portion of the scratch on Poco Graphite sample using 12.5 $\mu$ m diamond stylus.....	48
4.15: Force and AE plot for starting portion of the scratch on Poco Graphite sample using 12.5 $\mu$ m diamond stylus.....	48
4.16: Wyko image of DBT depth for Poco Graphite sample scratched using 12.5 $\mu$ m diamond stylus.....	49
4.17: Force and AE plot of DBT depth for Poco Graphite sample using 12.5 $\mu$ m diamond stylus.....	49
4.18: <i>Wyko image showing the brittle fracture after the DBT region on</i> Poco Graphite sample using 12.5 $\mu$ m diamond stylus.....	50
4.19: Optical image showing ductile to brittle transition of the Poco Graphite sample using 12.5 $\mu$ m diamond stylus.....	50
4.20: Apparent Coefficient of friction for Poco Graphite sample polished at less than 100 nm (Ra) from scratching experiment using 5 $\mu$ m stylus.....	51
4.21: Apparent Coefficient of friction for Coors Tek sample polished at less than 10 nm (Ra) from scratching experiment using 12.5 $\mu$ m stylus.....	51
4.22: SEM image of a 5 $\mu$ m worn/broken diamond stylus tip.....	53
4.23: SEM image of the tool edge corner from flat nose tool used for inclined plane experiment of Poco Graphite sample .....	53
4.24: SEM image of a 12.5 $\mu$ m tip radius diamond stylus.....	53

## List of Figures — Continued

5.1: Experimental setup for SPDT of CVD SiC .....	57
5.2: Picture showing the optical quality of the surface finish on the machined CVD SiC sample .....	59
5.3: CAD model showing the surface roughness distribution for 6 inch CVD SiC plate .....	59
5.4: Optical images comparing CAD drawing.....	60
5.5: Wyko images comparing the surfaces before and after machining .....	60
5.6: Optical microscope image of tool edge after machining .....	61
5.7: Comparison of depth and surface roughness data .....	62
5.8: Optical image of the machined surface showing the actual feed/rev for region 1 .....	63
5.9: Schematic showing a sectional view of the 6 inch plate comparing the step size for depth of cuts .....	63
5.10: Chart showing the surface roughness achieved for different samples after each pass of machining .....	65
6.1: <i>Picture showing the Quartz (Infrasil 302) used for scratches</i> .....	66
6.2. Wyko image for the scratch showing the DBT depth of Infrasil 302 using 5 $\mu$ m stylus .....	68
6.3. Force plot for the scratch showing the DBT depth of Infrasil 302 using 5 $\mu$ m stylus .....	68
6.4: Wyko image showing the brittle fracture zone after the DBT depth of Infrasil 302 using 5 $\mu$ m stylus .....	69
6.5: Schematic representation of the experimental setup for inclined plate experiment .....	70



## List of Figures — Continued

6.6: Wyko image showing DBT depth for scratch on Infrasil 302 from inclined plate experiment.....	70
6.7: Force plot for DBT depth of scratch on Infrasil 302 from inclined plate experiment .....	71
6.8: Wyko image showing the brittle region of the scratch on Infrasil 302 from inclined plate experiment .....	71

## CHAPTER 1

### INTRODUCTION

Ceramics have been used since the earliest civilization. The field of ceramic materials has its roots in more traditional aspects of the subject like clay based ceramics and glasses. However, during the past few decades, new developments in the use of ceramics in more advanced technological applications have attracted considerable attention. Ceramics are defined as solid compounds that are formed by the application of heat and sometimes heat and pressure. Ceramics are comprised at least two elements provided one of them is a non-metal or a non-metallic elemental solid. The other element(s) may be metal(s) or another non-metallic elemental solid(s). A somewhat simpler definition was given by Kingery <sup>[1]</sup> who defined ceramics as, “the art and science of making and using solid articles, which have as their essential component, and are composed in large part of, inorganic nonmetallic materials.”

The increasing use of ceramics in advanced technological applications has resulted in a heightened demand for improvements in material properties and reliability. In recent years there has been a realization that these improvements can be achieved through careful attention to the fabrication processes used for different manufacturing requirements of ceramics. There has been a remarkable growth in fundamental and applied research in the field of ceramics to meet the requirements of these advanced technological applications.

## 1.1. Silicon Carbide

Ceramics consist of a host of different materials with special properties. Silicon Carbide (SiC) is one such material which is also known as carborundum or moissanite (the commercial name for silicon carbide when used as gems). SiC was accidentally discovered by Edward G. Acheson<sup>[2]</sup>, an assistant to Thomas Edison, about 1890, when he was running an experiment on the synthesis of diamonds. Acheson thought the new material was a compound of carbon and alumina, present in the clay, leading him to name it carborundum, a name that is still being used on some occasions. SiC occurs naturally in meteorites, though very rarely and in very small amounts. Being the discoverer of SiC, Acheson was the first to synthesize SiC by passing an electric current through a mixture of clay and carbon. Nowadays, SiC is still produced via a solid state reaction between sand (silicon dioxide) and petroleum coke (carbon) at very high temperatures in an electric arc furnace. A purer product is produced with different advanced manufacturing processes. SiC, as a technical ceramic, is produced in two main ways. Reaction bonded SiC is made by infiltrating compacts made of mixtures of SiC and C with liquid Si (such as Poco Graphite samples). The silicon reacts with the carbon forming SiC. The reaction product bonds the SiC particles. Sintered SiC is produced from pure SiC powder with non-oxide sintering aids (such as Coors Tek sample). Conventional ceramic forming processes are used, and the material is sintered in an inert atmosphere at temperatures of 2000°C or higher. Also single crystal SiC (such as samples made in CREE Inc.) is produced for semiconductor application. But this form of SiC is not included in this study.

SiC is special due to its ability to perform at high temperatures and its high wear resistance. There are other mechanical properties which are listed below which enhance the use of such a material. Typical characteristics include:

- Low density
- High strength
- Good high temperature strength
- Oxidation resistant
- Excellent thermal shock resistance
- High hardness and wear resistance
- Excellent chemical resistance
- Low thermal expansion and high thermal conductivity
- Electrical conductivity

The above special properties do make SiC appropriate for usage in high temperature applications such as engine components for automobiles. High wear resistance and a low coefficient of friction increases the durability of components produced using SiC. The low density and high strength decreases the component weight which in turn decreases the complete product weight. The usage of SiC for engines in automobiles is at an initial stage now, such as water pump seals, but there are some applications listed below for which SiC is being widely used.

- Fixed and moving turbine components
- Seals, bearings, pump vanes
- Ball valve parts
- Wear plates

- Heat exchangers
- Semiconductor wafers
- Optical Mirrors

The use of SiC has increased researchers' curiosity towards other manufacturing processes which would open up avenues for new products.

## 1.2. Polycrystalline Silicon Carbide

Poly crystalline solids are merely a packed mass of small crystals (grains), so the characteristic shape may be partly reflected in the larger mass, or lost completely.

In the flow chart below figure 1.1 is shown the fabrication of poly crystalline ceramics (e.g. SiC) from powders which is known as the sintering process, the processing is divided into two parts: process prior to the firing of the green body and those that occur after firing. Each step has the potential of producing undesirable micro-structural flaws in the body that can limit material properties and reliability.

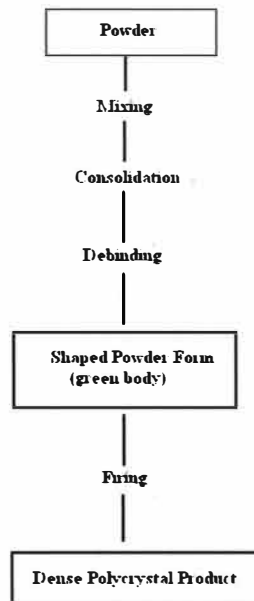


Figure 1.1. Flow chart for production of polycrystalline SiC by firing of consolidated powders

### **1.3. CVD Coated Silicon Carbide**

Until recently, the only commercially available polycrystalline silicon carbide has been sintered or reaction bonded hexagonal alpha silicon carbide. Design engineers have had to contend with the fact that the traditional powder consolidation process produces two-phase materials, i.e., some reaction bonded SiC contains as much as 40% free silicon. The "impurity" materials such as free silicon act to compromise the true performance of the SiC. CVD coated SiC (typically a coating of CVD SiC on a SiC substrate) is an excellent reflective optics material, exhibiting superior polishability with low scatter, exceptional thermal and cryogenic stability and high resistance to atomic oxygen and electron beam degradation. CVD coated SiC materials are used as substrates for fabricating mirrors for surveillance, high energy lasers (such as airborne laser), laser radar systems, synchrotron x-ray, VUV telescopes, large astronomical telescopes and weather satellites. CVD coated SiC lightweight mirrors can be produced either by conventional fabrication, near-net-shape fabrication and precision machining.

CVD coated SiC is a unique free standing, monolithic material with superior characteristics in terms of purity (>99.9%), homogeneity, density (99.9% dense), chemical and oxidation resistance, cleanability, polishability and thermal and dimensional stability. More than a coating, solid, cubic (beta) silicon carbide clearly offers performance advantages over other SiC material produced by traditional (sintering or reaction bonding) processes for applications including semiconductor processing equipment, optics, wear parts and heat sinks for electronic packaging. Because this material has a cubic beta structure, it also offers isotropic characteristics <sup>[3]</sup>. Hundreds of

tests conducted over the past several years confirm the material's homogeneity - not only within a production run, but also from batch to batch.<sup>[3]</sup>

#### **1.4. Conventional Manufacturing**

The usage of SiC is expensive due to expensive manufacturing costs. Processes like surface grinding produce subsurface fracture damage in the material. Complete removal of sub-surface fracture damage is possible through processes like polishing and lapping. These additional processes increase the final cost of the product, as polishing and lapping increase the cost of manufacturing by not less than 50% <sup>[19]</sup>.

##### **1.4.1. Lapping:**

In lapping, free abrasive is introduced between a lap, which may be a cast iron plate, and the work-piece surface. The free abrasive is usually suspended in a liquid medium, such as oil, providing lubrication and helping to transport the abrasive. The lap and the abrasive are both subject to wear. To maintain the required geometry of the lap and the work-piece surface, it is necessary to pay careful attention to the nature of the motions involved in order to average out the wear across the surface of the lap. Several laps may be employed and periodically interchanged to assist this process.

##### **1.4.2. Polishing:**

Polishing, like lapping, also employs free abrasive. In this case, pressure is applied on the abrasive through a conformable or soft cloth or pad. This allows the abrasive to follow the contours of the workpiece surface and limits the penetration of individual grains into the surface. Polishing with a fine abrasive and a flexible pad creates a very gentle abrasive action between the grains and the workpiece, thus ensuring a very small grain penetration depth, i.e. low scratch depths.

The main purpose of polishing is to modify the surface texture, produce a smooth surface, rather than change the shape. Highly reflective mirror surfaces can be produced by polishing. The material is removed at a very low rate. Consequently, the geometry of the surface needs to be very close to the correct shape before polishing is commenced and low material removal preserved the form and shape.

Optimization of cost is possible with the introduction of machining, which could replace processes like finish grinding, polishing and lapping. This could result in cheaper products, enhancing the commercial use of materials like SiC.

### **1.5. Precision Machining**

The primary idea of using precision machining is to use displacement controlled cuts to generate the required surface shape. Precision machines are used to machine under controlled speeds, feeds and depth of cuts. Precision machining using a Universal Multi-Test system (Tribometer), has recently been demonstrated (ref: Proceedings of HPPT workshop 2005, Knoxville, TN <sup>[24]</sup>), which is primarily used for precision tribological experiments, e.g., wear tests and friction tests. The major difference between a precision diamond cutting machine and a tribometer is that the tribometer is load controlled but the precision diamond cutting machine is displacement controlled.

Ductile removal of ceramic and semiconductor material is possible due to a high pressure phase transformation which is achieved by machining materials like SiC at the nano-scale. To achieve such results, use of precision diamond turning machines, or a device similar to UMT Micro-Tribometer, along with precision diamond tools is necessary. Due to their high controllability, precision machines can be used for form tolerances in nanometer size range. The use of machining has proved useful to remove



surface flaws generated due to grinding process, as precision machining also could replace processes like grinding, polishing and lapping, decreasing the manufacturing cost and cycle time.

## **1.6. Project Goals**

In view of achieving ductile cuts on materials like SiC, different kinds of SiC were evaluated. One is polycrystalline SiC (Coors Tek Inc.) and the other is CVD coated SiC (Coors Tek Inc. and Poco Graphite Inc.). Polycrystalline SiC was used for orthogonal cutting using a diamond turning machine (single point diamond turning, SPDT). DBT depths were determined for CVD coated SiC by scratching on the surface using a diamond stylus. This was followed by diamond turning of CVD coated SiC using a tribometer. The goals for the first set of experiments using polycrystalline SiC were as follows:

- Record and analyze the machining forces with respect to the different depth of cuts (10 and 25nm)
- Map surface roughness values with change in depth of cuts
- Determine tool wear and compute ratio of volume of tool wear and volume of material removed

The goals for CVD coated SiC were as follows:

- Determination of ductile to brittle transition depths for two different makes of material, one from Poco Graphite and the other from Coors Tek
- Develop process parameters for diamond turning of CVD coated SiC
- Achieve diamond turning of a 6 inch diameter CVD coated SiC plate with surface finish of <65nm (mirrors- application)

- Optimize tool wear by use of cutting fluids

This thesis discusses all experiments performed on SiC to achieve ductile mode machining. Chapter 2 covers the research background which is a base for this study. Chapter 3 covers the ductile regime machining of polycrystalline SiC. In chapters 4 discusses the experiments to determine the ductile to brittle transition depths of CVD coated SiC and chapter 5 covers the experiments which would show the accomplished diamond turning of a 6inch CVD coated SiC plate will be discussed. Chapter 6 covers the determination of a ductile response and the determination of DBT depth for quartz (Infrasil 302). Chapter 7 summarizes the conclusions of the thesis and also provides suggestions for future work.

## CHAPTER 2

### BACKGROUND OF RESEARCH

Understanding ductile mode machining is beneficial for faster and economical processing of brittle materials. Over the past 20 years there has been extensive study of indentation, scratching, grinding, machining and similar operations to explore the machinability of materials like silicon, silicon carbide, silicon nitride, germanium, glass and similar materials. This previous research was conducted to understand the process parameters and feasibility of the different manufacturing processes. This chapter deals with work done by different researchers regarding ductile mode machining of brittle materials and the theory that supports similar research for such materials.

#### **2.1. Origin of Ductility**

Single point diamond turning was first developed for the production of optical components from non-ferrous metals such as aluminum and copper. As the need for infrared optics grew, the technology was adapted to brittle materials like Si and Ge <sup>[4]</sup>.

Morris and Patten <sup>[5]</sup> in their results provide insight to the origins of the ductile regime during single point diamond turning of semiconductors, for which optically smooth surfaces can be produced. Both the machined chips and finished surface was studied under TEM. The deformation mechanisms responsible for material removal were presented and compared to plastic mechanisms of deformation that occur in low load indentation and micro-scratching experiments. The morphological character of the chips showed evidence of high ductility with no evidence of molten flow. They concluded that structurally the chips are amorphous and contain varying amount of micro-crystalline

fragments. The amorphous phase that is seen in the chips is not due to oxidation; rather it is likely the end result (back transformation) of a pressure induced phase transformation.

Bifano et al. [6] predicted irreversible material-removal mechanisms can be divided into two types: brittle and ductile. In brittle fracture mechanisms, material removal is accomplished through the propagation and intersection of cracks, while ductile mechanisms produce plastic flow of material in the form of severely sheared machining chips. The results of their investigation included an immense research effort to characterize the physical parameters that control the brittle to ductile transition in grinding of brittle materials. The final results of their research suggested strong evidence of ductile mode grinding of brittle materials.

A model was proposed defining the brittle to ductile transition depth in terms of the material properties of the work-piece and the material removal rate by Bifano et al. [6] To investigate the influence of material properties on the DBT critical depth, a broad range of amorphous glass, single crystals, and advanced ceramics were chosen for grinding experiments. By comparing the grinding ductility of these materials to their intrinsic properties, a critical depth of cut model was established. Based on Griffith fracture propagation criterion, this formula predicts a critical depth of cut:

$$d_c = (E.R) / H^2 \dots\dots\dots(2.1)$$

where  $d_c$  is the critical depth of cut,  $E$  is the elastic modulus and  $R$  is the fracture energy,  $H$  is the hardness. The value of  $R$  can be evaluated using the relation:

$$R \sim K_c^2 / H \dots\dots\dots(2.2)$$

The quantity can be combined to represent the critical depth as

$$d_c \sim (E / H). (K_c / H)^2 \dots\dots\dots(2.3)$$

as a measure of the brittle transition depth of cut. In spite of a few problems with determining the material properties, a reasonable correlation was obtained by Bifano et al. between the calculated critical depth of cut and the measured depth or the grinding infeed rate (i.e the grinding infeed that will produce 10 % surface fracture). From this correlation the constant of proportionality was estimated as to be 0.15 in Eq.(2.4):

$$d_c \sim 0.15 \cdot (E / H) \cdot (K_c / H)^2 \dots\dots\dots (2.4)$$

## 2.2 Phase Transformation

Gogotsi et al.<sup>[7]</sup>, and Patten and Gao<sup>[8]</sup> stated in their work that the occurrence of high pressure phase transformations of semiconductors and ceramics is often characterized by the amorphous remnant that exists, on the surface and within the chip, after processing. This amorphous remnant is a result of a back transformation from the high pressure phase to the atmospheric pressure phase due to rapid release of pressure in the wake of cutting tool, i.e., the high pressure phase only exists when the pressure is applied, when the pressure is released the material reverts to another phase. The rate at which the pressure is released, along with the maximum pressure imposed, can also affect the resultant back transformed phase. It is believed by the authors that a high pressure phase transformation and/or amorphization of SiC is responsible for the observed ductile machining behavior, as has been found with other hard brittle materials such as silicon, germanium and silicon-nitride.

Yoshida et al.<sup>[9]</sup> in 1993 performed X-ray diffraction studies for cubic (3C) and hexagonal (6H) polytypes of SiC under pressures of 105 and 95 GPa respectively, using a diamond anvil cell and an imaging plate technique. 3C- SiC undergoes a phase transition into the rocksalt type structure at 100 GPa accompanied by a volume reduction of 20.3%.

The 6H polytype of SiC remains stable to the highest pressure studied, with a promotion of a phase transition above 90 GPa. Equation of state data for the two polytypes has been found to be essentially the same to 95 GPa, yielding the bulk modulus 260 GPa .

Raman scattering analysis of single point diamond turned Si by Pizani et al. <sup>[10]</sup> revealed the amorphization of Si surfaces, contrary to brittle mode machining conditions, where this amorphous layer does not exist. This amorphization process was attributed to the pressure –induced phase transformation generated by the hydrostatic pressure and imposed by the cutting tool tip during machining. This fact suggests that the ductility of a fragile material such as Si can be correlated to the phase formation. Raman scattering analysis revealed that the shortening of phonon correlation length indicates that at the vicinity of the surface, this layer is composed of Si crystallites immersed in a amorphous Si media.

### **2.3. Material Removal / Chip Formation**

Scattergood and Blake <sup>[11]</sup> predicted that with the advent of high stiffness, high precision machine tools it is now possible to machine brittle materials without introducing subsurface fracture damage. This limit has been termed as “ductile-regime” machining. The profile of the uncut chip (Figure 2.1.) in a machining operation is central to the understanding of the subsurface damage produced. Chip profile geometry will interplay with the material removal mechanisms such that the damage left in the part will be controlled by both the geometry and material response. The latter can be characterized as a critical depth of cut for the onset of ductile to brittle fracture transition. Also important is the size scale of the fracture damage produced at this transition depth.

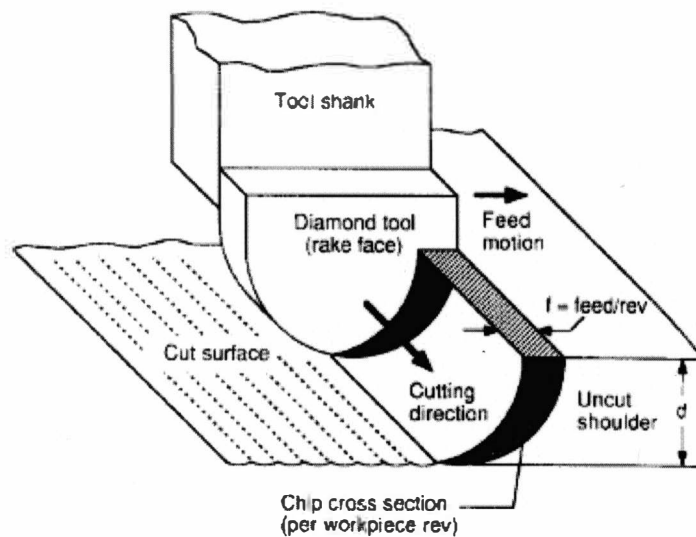


Figure 2.1: Chip profile geometry for single point machining using a round nose cutting tool <sup>[11]</sup>

Nakasuji et al. <sup>[12]</sup> described the chip removal process of brittle materials as being either brittle or ductile. Ductile chip removal conceptualized as a result of plastic deformation on the characteristic slip plane, or possibly via an amorphization process. Brittle chip removal is the result of cleavage fracture on the characteristic cleavage plane. Ductile chip removal produces a very smooth surface where as brittle chip removal produces a surface covered with residual pits and cracks. Both types of material removal are described as a function of the magnitude of stress field located at the tool tip and workpiece interface. An illustration of this stress field is shown in figure 2.2.

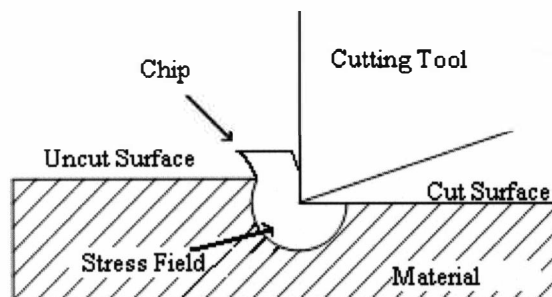


Figure 2.2: Stress field generated in a chip

Blake and Scattergood<sup>[11]</sup> also suggested a model for micro-fracture damage transitions at the chip and within the stress field region for ductile regime machining. They developed a model that describes for a given machining parameters, a critical cutting depth or critical chip thickness ( $t_c$ ) below which fracture damage does not occur on a finished surface. When  $t_{eff}$  (effective chip thickness)  $< t_c$ , ductile response occurs along the tool nose radius, whereas when  $t_{eff} > t_c$ , fracture occurs, resulting in micro-fracture damage zone shown schematically in figure 2.3.

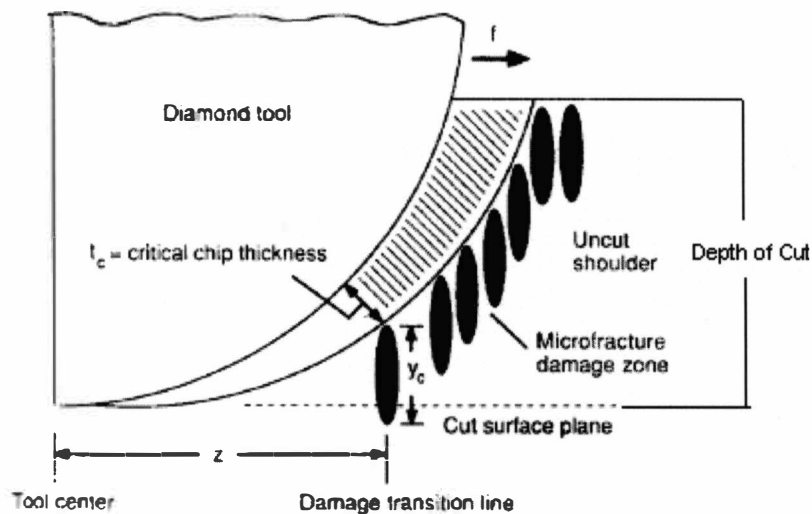


Figure 2.3: Model of micro-fracture damage transitions in ductile regime machining<sup>[11]</sup>

As soon as the micro-fracture damage zone of depth  $y_c$ , produced at  $t_c$ , penetrates below the cut surface shown in figure 2.3 the finished surface will contain micro-fracture pitting damage and machining conditions have then moved out of the ductile regime. Ductile regime is by no means a mode where the material is totally removed in a ductile fashion. Material removal in the uncut shoulder above  $t_c$  (or above  $y_c$ ) in Fig.2.3 occurs by a combination of plasticity and extensive micro-fracture. Hence Scattergood and Blake concluded that ductile regime machining is an interplay between tool profile



geometry, feed and depth of cut, which determine the chip cross-section and a critical depth parameter  $t_c$  that dictates fracture initiation.

## **2.4. Surface Characteristics**

Fritz Klocke et al. in Jahanmir's book about machining of ceramics <sup>[13]</sup> described experiments to correlate machining parameters to the surface roughness. Various unsintered and presintered oxide and carbide ceramic materials were machined. In his experiments, cone turning was used to determine which machining conditions were suitable for turning operations. It was found that in the case of presintered SiC, the surface quality at high feed rates deteriorates; this correlation was examined for different infeeds. It became evident that at smaller cross feed rates the surface finish becomes independent of the infeed ( $t < t_c$  or  $y < y_c$ ). Apparently a limit exists for the chip formation forces acting on the surface, below which there is no noticeable change in the extent of fracture (i.e. no fracture), and therefore of roughness becomes independent of depth.

Yin et al. <sup>[14]</sup> in his work on surface characterization of 6H-SiC did foresee that the requirements for final surface finish of SiC wafers are very stringent, the final roughness in terms of root-mean-square ( $R_q$ ) should be on the nanoscale. For epitaxial growth and electronic device fabrication, atomic flatness, i.e. sub-nanometer roughness, is preferred. Yin et al performed indentations, and grinding followed by polishing tests on 6H-SiC substrates for different grit sizes of diamond wheel. The results showed dependency of surface roughness on the grinding speed and grit size. In this study, the results showed that there was a true scale effect for material deformation and removal

mechanisms in indentation and abrasive machining of the single crystal 6H-SiC (0001) substrates. Also, the process of material removal in abrasive machining followed the same micro-fracture and deformation events as observed in indentations. This suggests that although the abrasive machining with diamond abrasives is different dynamically, thermally and geometrically from the deformation produced using quasistatic indentations, there are essential similarities in both processes with respect to material deformation.

## **2.5 Effect of Rake Angle and Cutting Edge Radius of the Tool**

The design of tools used for machining of brittle materials does affect the end results, i.e. the DBT. Considerable research has been done to study the effect of rake angle on the machining of brittle materials.

Blackley and Scattergood <sup>[4]</sup> conducted experiments on machining of germanium with  $0^{\circ}$ ,  $-10^{\circ}$  and  $-30^{\circ}$  rake angle tools. They found that the critical depth of cut for germanium increased with (each successive) more negative rake angle. Shibata et al. <sup>[15]</sup> diamond turned single crystal silicon with both  $-20^{\circ}$  and  $-40^{\circ}$  rake angle tools. At a 100nm depth of cut the  $-40^{\circ}$  rake tool produced a purely ductile surface finish.

Patten and Gao <sup>[8]</sup> performed experiments with a unique method of varying the tool's rake angle; the center line of the tool's cutting edge was adjusted to create an effective negative rake angle from 0 degree to 90 degrees. At the midpoint between these two extremes, the effective rake angle is  $-45^{\circ}$  other effective rake angles such as  $-15^{\circ}$ ,  $-30^{\circ}$  and  $-60^{\circ}$  deg, were also available. As the rake angle is decreased from 0 to  $-45^{\circ}$  deg, the relative amount of ductile cutting increases and the brittle fracture contribution decreases.

Also the cutting mechanism transitions from a more ductile to a more brittle behavior as the depth of cut is increased from 100nm to 500nm.

Fang et al <sup>[29]</sup> reported that the cutting edge radius,  $r$ , can also have a significant effect on the DBT. The cutting edge radius can be considered sharp as long as the depth of cut is larger than the edge radius. If the depth of cut is less than the edge radius then an effective rake is created. In this situation a  $0^\circ$  rake produces a negative rake and a negative rake produces a more negative rake. An effective rake angle created with a negative rake produces a more negative rake. An effective rake angle created with a negative rake tool can lead to an excessive negative rake. Fang et al <sup>[29]</sup> suggested that excessive rake can create excessive pressure that can mar the surface.

## 2.6. Tool Wear

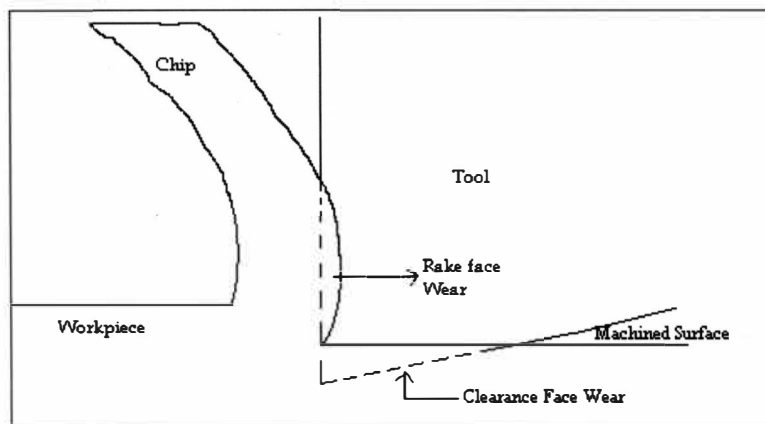


Figure 2.4: Schematic model showing wear of the tool<sup>[16]</sup>

To understand the role of tool wear in surface quality degradation, Hurt and Decker <sup>[16]</sup> had proposed that there are two types of tool wear: rake face wear and clearance face wear. The action of the chip rubbing as shown in Fig 2.4 causes the rake face wear and contact with the machined surface causes a clearance face wear. High compressive stresses exist on the rake face of the tool and are at a maximum at the cutting edge. Compounding this effect is the possibility of high temperature, at high

cutting speeds/velocity on the rake face due to sliding friction of the chips and high strain rates.

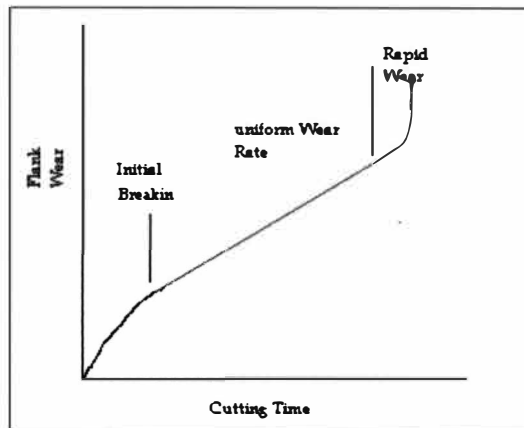


Figure 2.5: Flank wear vs machining time<sup>[16]</sup>

The progression of clearance wear is shown in Fig: 2.5. After an initial rapid breakin of the cutting edge, a uniform wear rate is established. The tool needs to be resharpened when the wear reaches its deterioration phase (rapid wear). For the production of high quality optical surfaces, tool wear generally increases the surface roughness value.

Preliminary research in machining single crystal silicon with a worn tool was done by Jasinevicius et al. <sup>[17]</sup>. Possible wear mechanisms affecting tool performance during cutting were discussed. SEM and AFM images of the tool and the surface were analyzed to study the wear patterns. Their research showed that worn tools can generate high stress levels with an increase of penetration depth. If the compressive stresses are high enough, and the tensile stresses low enough, the onset of the phase transformation and then plastic deformation takes place prior to cracking. The rapid and deleterious wear of the diamond tool when cutting silicon and presumably ceramics is considered a constrain factor in the production of large surfaces.

## 2.7. Machining Forces

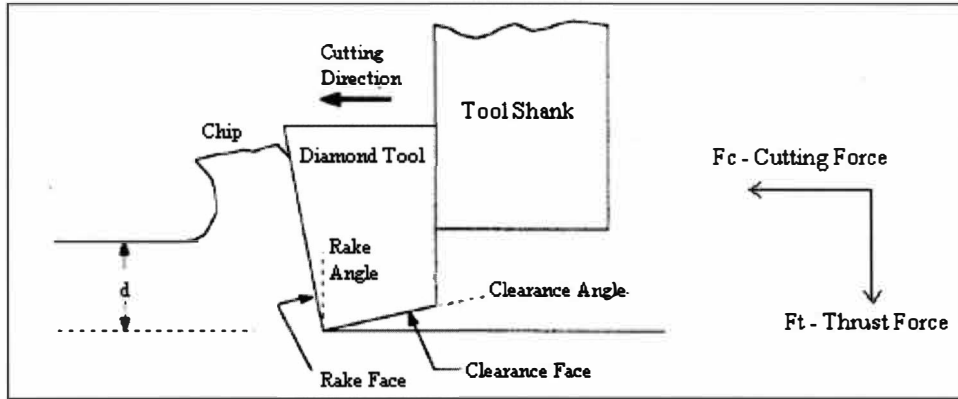


Figure 2.6: Schematic of orthogonal cutting model showing the direction of forces<sup>[11]</sup>

Machining of brittle materials produces forces in the form of cutting force  $F_c$  and thrust force  $F_t$  (figure 2.6). Research done in the past on machining of brittle materials has established a relationship between machining forces and ductile mode machining. The machining forces monitored are also used for calculating the coefficient of friction. The coefficient of friction is typically less than 1. The frictional behavior is represented as Eq.2.5:

$$F_f = \mu \times F_n \dots \dots \dots (2.5)$$

where the cutting force  $F_c$  represents the friction force  $F_f$  and thrust force  $F_t$  is represented as normal force  $F_n$ . The value of COF could be greater than 1 which is known as the apparent coefficient of friction ( $\mu_a$ ). Typically while machining at larger depths when the cutting forces become higher than the thrust forces, the apparent coefficient of friction comes into existence.

Patten and Gao <sup>[8]</sup>, for the purpose of discussion and with regard to machining forces state that, high forces are considered to be indicative of ductile machining and lower forces are considered to be due to brittle material removal for a given depth of cut.

It generally takes less energy (lower forces) to remove material via brittle fracture than by ductile or plastic deformation on a per unit or volume basis, or at the same depth of cut.

The energy required for plastic deformation is directly proportional to the volume of the material removed; whereas the energy for brittle fracture is directly proportional to the crack surface area. The process requiring minimum energy will prevail. Dislocations or slip sites must be available for plastic flow (directly proportional to volume) and a suitable crack size/location must be available for fracture (directly proportional to surface area).

## CHAPTER 3

### DUCTILE REGIME NANO-MACHINING OF POLYCRYSTALLINE SILICON CARBIDE

#### 3.1. Introduction

In recent years, considerable progress has been made on the machinability of crystalline semiconductors, because of the demand for faster fabrication processes of complex surface shapes.<sup>[10]</sup> Advances in precision engineering have led to the discovery of a “ductile regime” mode of operation, for nominally brittle materials, in which the material removal is via plastic deformation.<sup>[10]</sup>

SiC experiences a ductile to brittle transition similar to other brittle materials, e.g. semiconductors and ceramics. It is believed that the ductility of SiC during machining is due to the high pressure phase transformation (HPPT) at the cutting edge of the tool, which encompasses the chip formation zone. The remnant of the HPPT can be seen, after ductile regime machining, in the finished machined surface and in the machining chips (debris). The chips are amorphous (in contrast to the starting polycrystalline structure), which reflects machining in the “ductile regime”. This amorphization of chips is due to the high pressure and shear generated at the contact between the tool and the SiC sample during machining. This chapter concentrates on the possibility for machining polycrystalline SiC in the ductile mode, which was performed at low speeds ( $< 1\text{m/s}$ ) and very low depths of cut ( $< 100\text{nm}$ ).

### 3.2. Experimental Setup for Machining of Polycrystalline SiC

The SPDT of the poly crystalline SiC was done on a diamond turning machine (DTM), as shown in Figure 3.1. The dimensions of the poly crystal 6H SiC tube (SC 30, Coors Tek, USA) used for the experiments are given in figure 3.2.

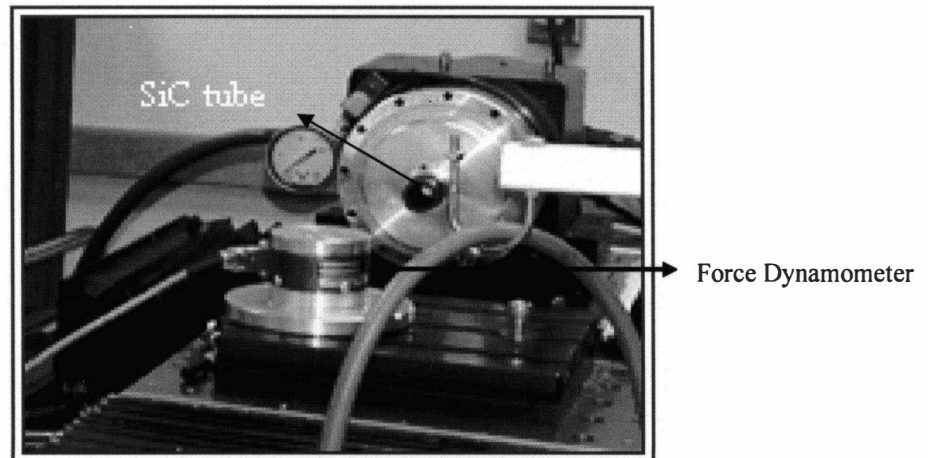


Figure 3.1. Experimental setup for machining of polycrystalline SiC

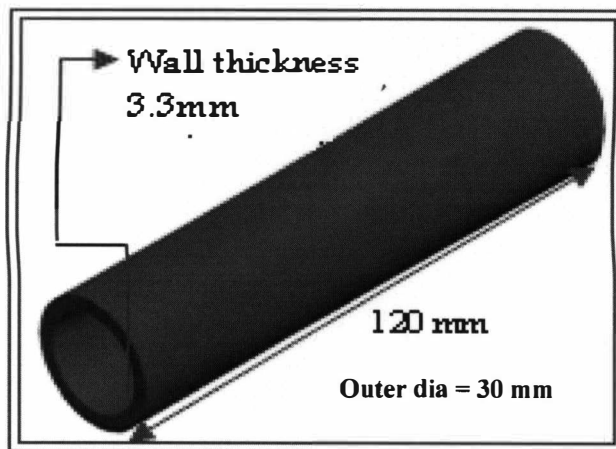


Figure 3.2. CAD drawing showing the specifications of the SiC tube

Poly crystal diamond tools and single crystal diamond tools were used for the experiments, the tools used were flat with a -45 degree chamfer, which served as the rake angle. The cutting edge radius (sharpness), of the single crystal diamond tools, was estimated at approximately 50nm, based upon manufacturer's information (the cutting edge was not measured prior to machining). To prepare for the 2D- orthogonal cuts, the wall thickness (3.3 mm) of the SiC tube was pre-machined using the poly crystal



diamond tool (plunge cuts with an infeed of 100nm/rev and up to 20 microns of total material removed). This was done to true up the SiC tube relative to the machine/fixture and tool/dynamometer. The rotational speed (RPM) of the DTM was initially maintained at 10 rpm (for the smallest depths/in-feeds), providing a very slow surface or cutting velocity of about 0.015m/sec. The speed was increased to 100 rpm or a cutting velocity of 0.15m/sec to avoid stalling the spindle at larger depths and feeds. This slow cutting speed results in low temperatures in the process or cutting zone, thereby minimizing the influence of thermal softening of the work piece material <sup>[8]</sup>.

During the cutting operations the thrust and the cutting forces were monitored through a calibrated, 3- axis dynamometer (JR3 Inc.). After each machining condition the chips were collected and the surface was inspected and surface roughness measured.

### **3.3. Results**

#### **3.3.1. Force Plots for Cutting and Thrust Forces for Different Cutting Tools:**

Figure 3.3 shows the increase in force with increase in depth of cut from 10nm to 25nm. The forces generated by different tools (Edge and Chardon tools) at the same depth of cut were comparable (figure 3.5). Figures 3.4 and 3.6 show the corresponding force ratios achieved from the cutting and thrust forces (figures 3.3 and 3.5). At low depths of cut, the thrust forces are always greater than the cutting forces, due to a significant role of the negative rake angle tools and due to rubbing (friction) against the flank face of the tool.

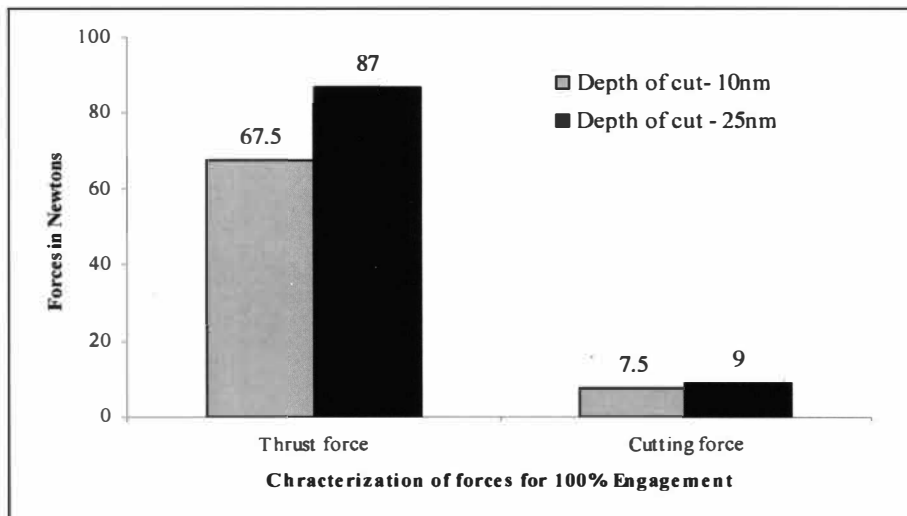


Figure 3.3. Comparison of forces for different depths of cut (Chardon tools)

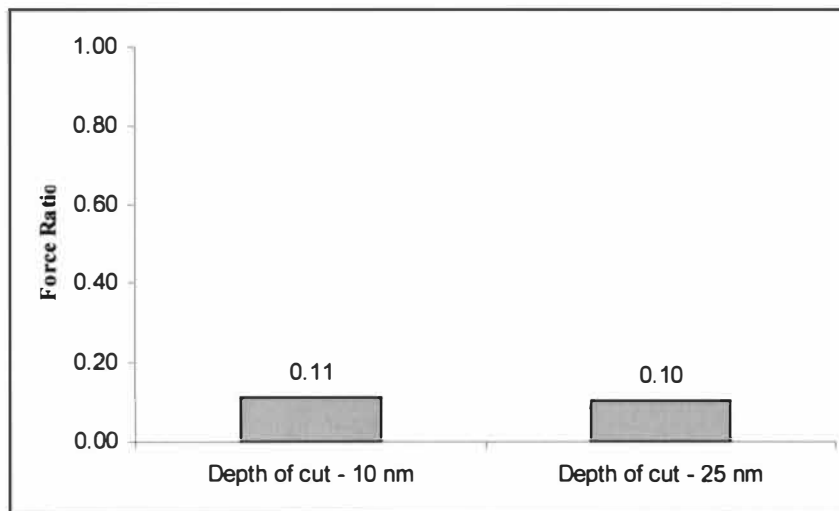


Figure 3.4. Comparison of force ratio for 10 and 25 nm depth of cuts

The force data was recorded through a force dynamometer and a LabVIEW interface. The electric force signals created by the force dynamometer were transferred to the computer. The LabVIEW program was created to capture the dynamometer force signal, print the signal to the computer screen and store the signal as text file. The goal was to acquire data points only when the tool was cutting. These text files were then imported in MS Excel and filtered to achieve the final required results.

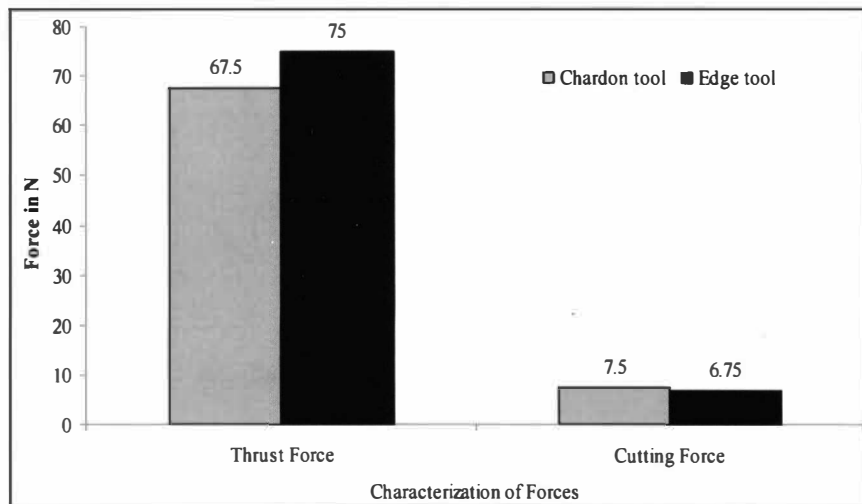


Figure 3.5. Comparison chart for forces achieved from Chardon and Edge tools at 10nm depth of cuts

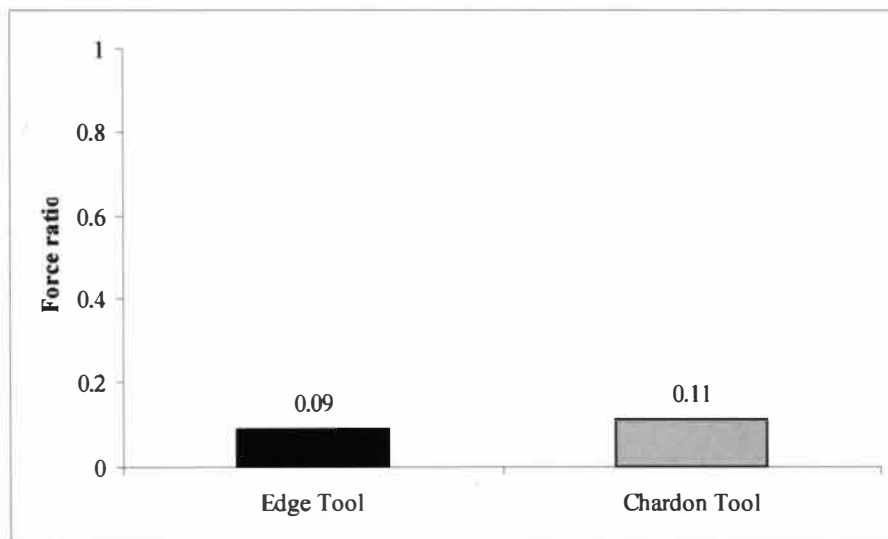


Figure 3.6. Force ratio for Chardon and Edge tool at 10 nm depth of cut

### 3.3.2. Surface Roughness:

The machined surface shows evidence of both ductile and brittle material removal, i.e. rough (brittle) and smooth (ductile) surfaces. The surface profiles for 10nm and 25nm cuts have been shown in Figure 3.7 (a), (b) and (c). The best surface roughness achieved for 10nm (Chardon tool) cuts was 62.5nm (figure 3.8) and for the 25nm (Edge tool) cuts was 46.8nm (figure 3.9). Best surface roughness achieved is limited by the grain size and polycrystalline nature of silicon carbide used, and the tool's cutting edge quality (edge radius, strength, defects or flaws). The surface roughness data was acquired from a surface profilometer (Taylor Hobson Form Talysurf 120 Stylus Profiler).

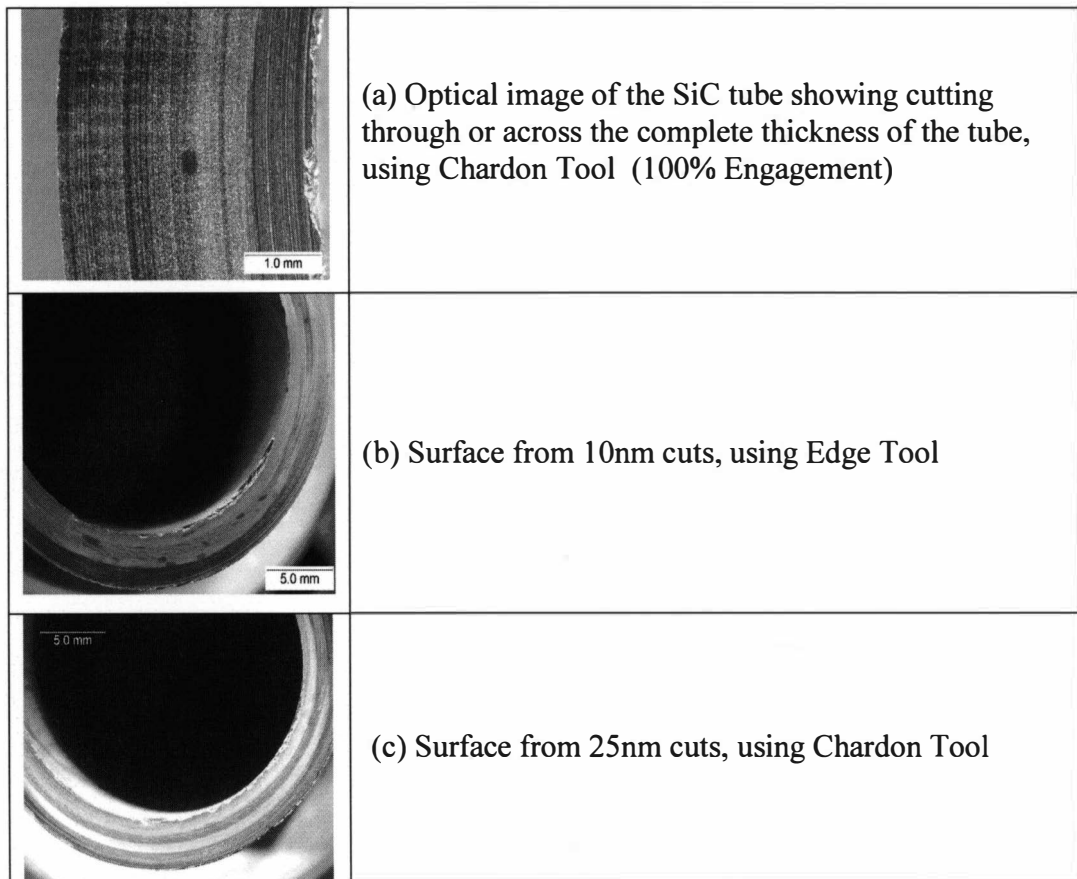


Figure 3.7: Surface profiles for the SiC tube after machining

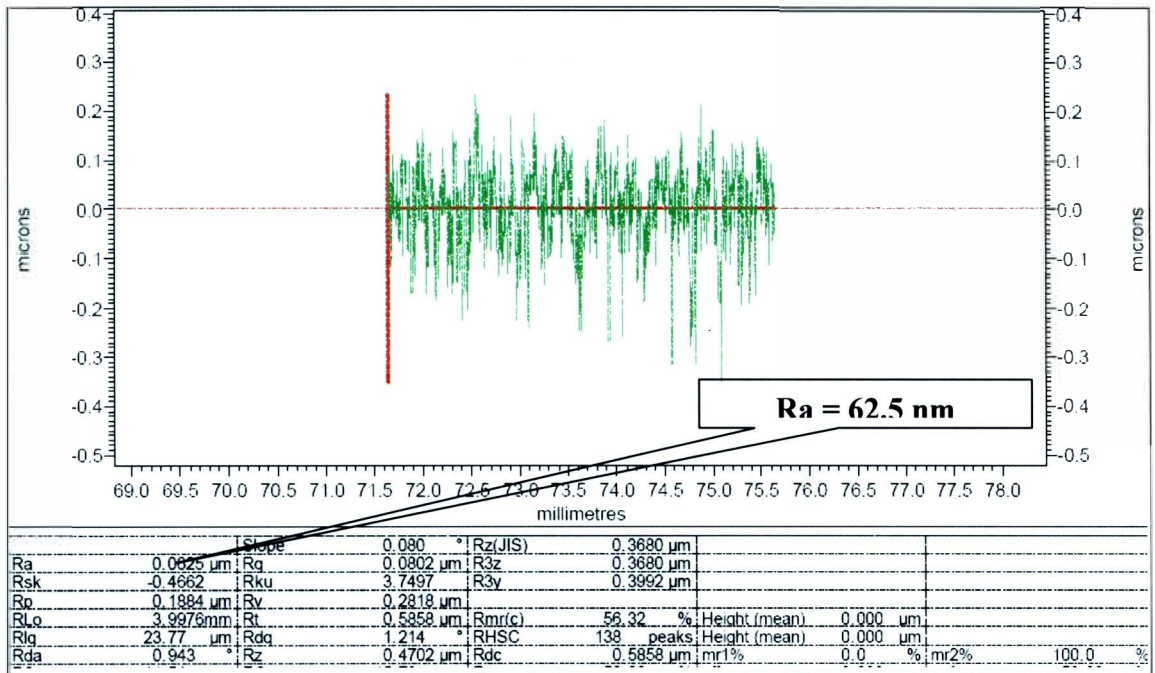


Figure 3.8: Surface roughness plot for 10 nm depth of cut showing the best surface roughness achieved

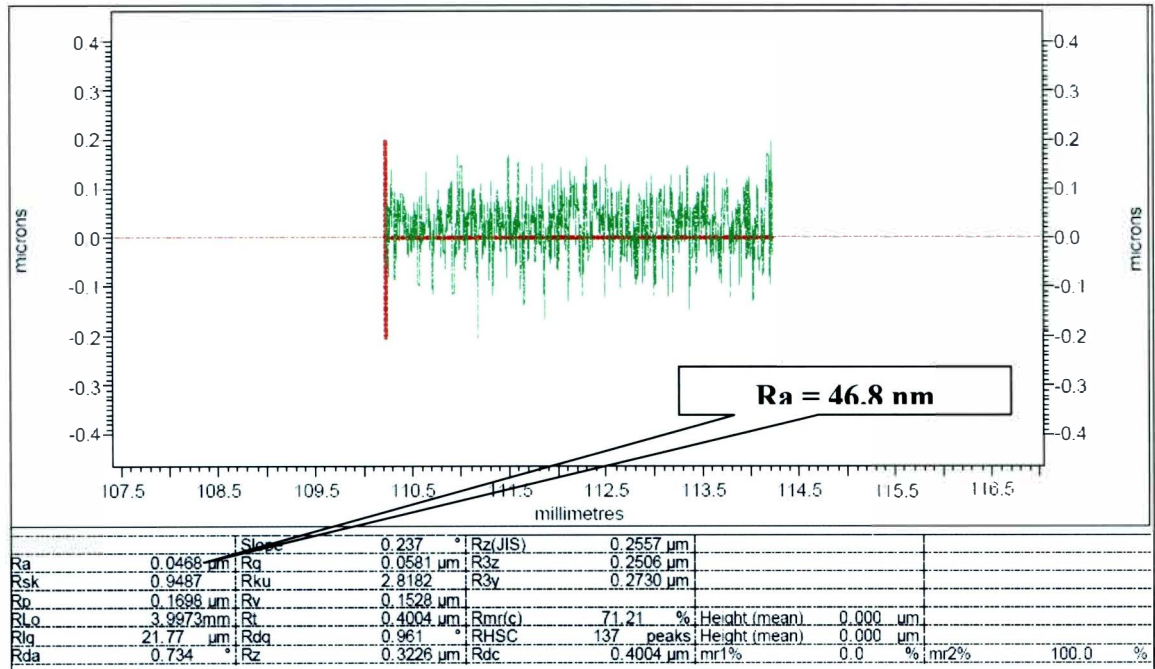


Figure 3.9: Surface roughness plot for 25 nm depth of cut showing the best surface roughness achieved

### 3.3.3. Tool Wear:

Tool wear is an important parameter to investigate for such experiments where the materials involved in machining are equally hard. As expected for these dry cuts, i.e. no machining/cutting fluid was used, there was significant tool wear. Tool wear was measured for the Chardon single crystal diamond tools that were used for machining. The tool wear was measured after machining  $600\mu\text{m}$  (total depth or in-feed) of poly crystal SiC by projecting the tool tip on an optical comparator. The length of the tool tip wear (along rake face) was  $60\mu\text{m}$ . This gives a ratio of 1:10 (length of tool wear: depth of material removed), from which can be determined that for every  $10\mu\text{m}$  machined the tool wears  $1\mu\text{m}$  (from the tool tip up the rake face). Presently a linear relationship is assumed for the tool wear.

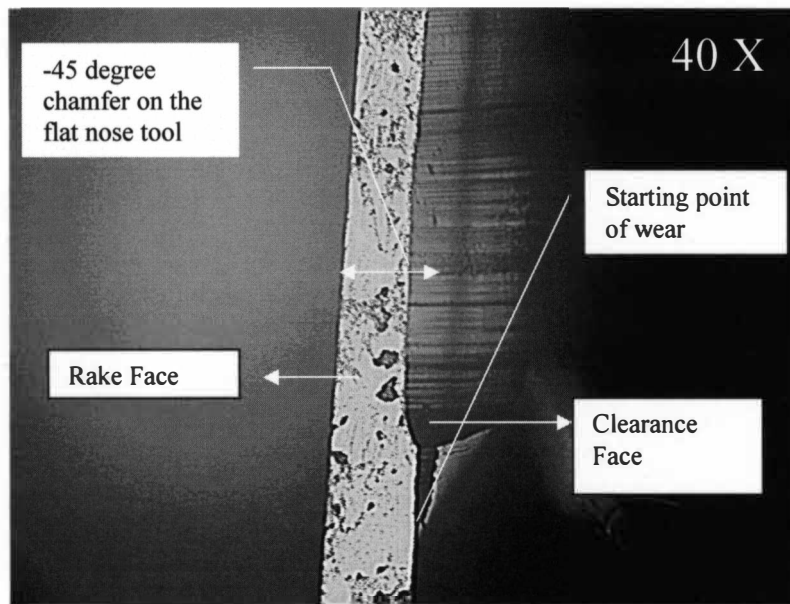


Figure 3.10: Optical microscope image of tool wear, the tool is at 45 deg to the microscope's lens, looking perpendicular to the rake face (Chardon Tool)

Analysis of the tool did reveal that wear was also prominent on the clearance face. The length of the clearance face wear was estimated to be  $370\mu\text{m}$  as shown in fig 3.11. This was revealed when the tool was viewed through an optical microscope fig 3.10. The tool wear ratio was calculated using simple geometry to be 1:182 (volume of tool wear: volume of material removed). This means that for every 182 cubic-microns of material removed the tool wears a corresponding 1 cubic-micron.

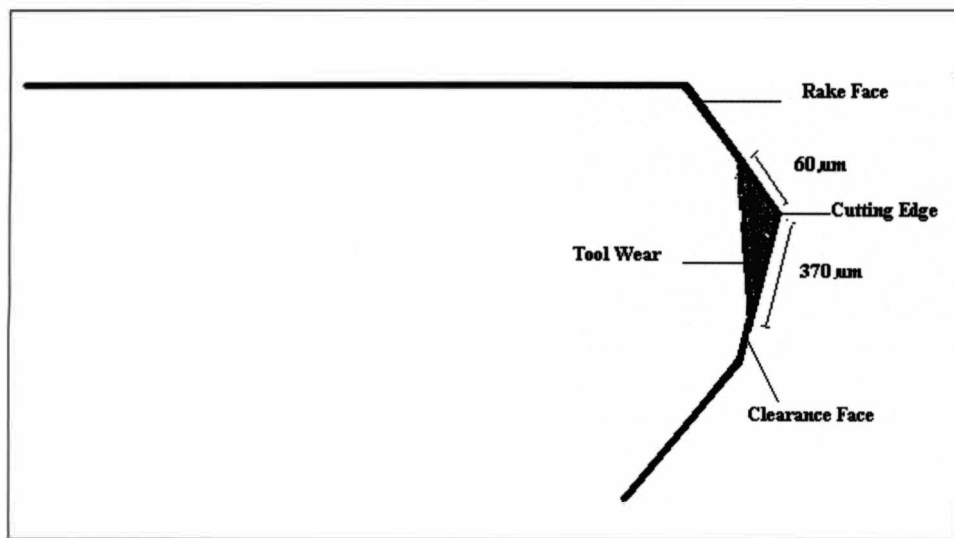


Figure 3.11. Schematic representation of tool wear

#### 3.3.4. Post Experimental Analysis:

The machining process produced both ductile and brittle chips. The ductile chips formed are relatively long and thin, and look like chips formed from metal machining. The brittle fracture chips are more like fragments, i.e. small pieces in the form of powder. Most of the brittle chips stick together forming agglomerates, which are extremely fragile. TEM observation confirmed the ductile nature of the chips and showed evidence of a phase transformation from crystalline to amorphous. The *ductile chips are amorphous*, as revealed by the amorphous ring of the electron diffraction pattern (for

example, fig 3.12). In addition to the longer amorphous chips, also found were the short crystalline debris that did not go through the apparent phase transformation. Electron diffraction indicated that the chips were 6H SiC. Thus some crystals in the original poly crystal material transformed into an amorphous structure, which has undergone significant ductile or plastic deformation during the machining process. These chips are seen in figure 3.13.

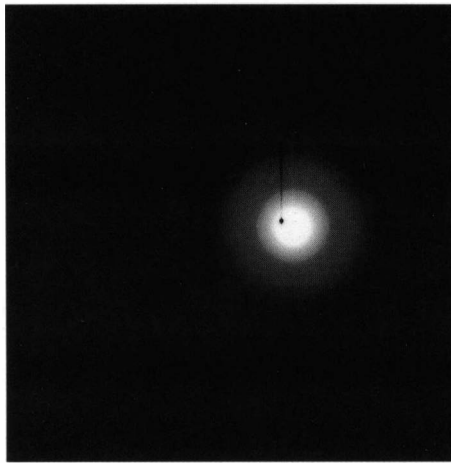


Figure 3.12. Image of diffraction pattern showing the halo ring for amorphous nature of the material (corresponding to the amorphous region shown in figure 3.13)

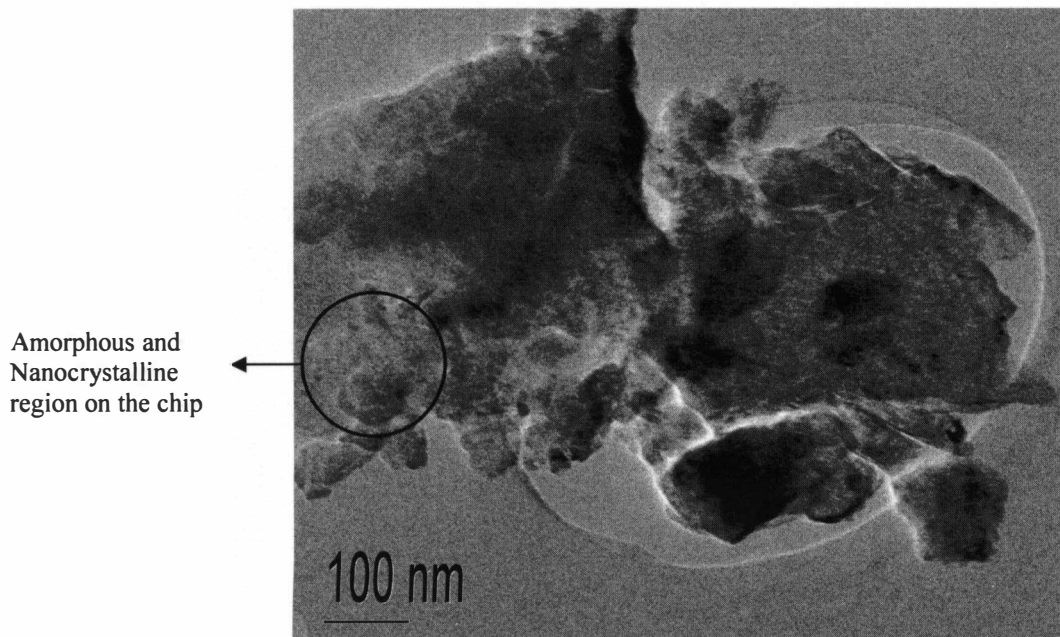


Figure 3.13. TEM image of a ductile chip from machining SiC



EDS evaluation (figure 3.14) during TEM indicates that the ductile chips are indeed SiC, as are the brittle debris. EDS evaluations show the presence of copper from the TEM grid.

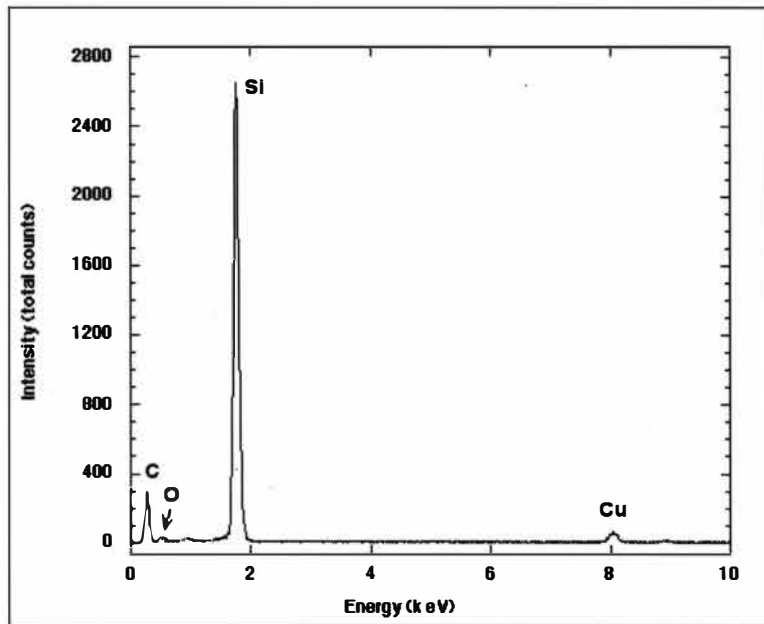


Figure 3.14. TEM EDS analysis of the ductile chip

### 3.4. Discussion

#### 3.4.1. Forces and Coefficient of Friction:

For the purpose of this discussion, the higher forces seen during machining rightly reflect ductile machining of poly crystal SiC. The lower forces show machining in the brittle regime, as less energy is required to machine brittle regions.

Due to the presence of friction forces, there is rubbing or plowing action during the machining process. The coefficient of friction,  $\mu$ , is typically  $< 1$ , as is the case for frictional behavior represented in equation below.

$$F_f = \mu * F_n \dots\dots\dots \text{Eq. (3.1)}$$

Where, the cutting force  $F_c$  corresponds to the friction force  $F_f$  and the thrust force  $F_t$  is represented by the normal force  $F_n$ . In the case of diamond on poly crystal SiC:  $\mu \approx 0.1$  [16] which is also comparable to the calculated force ratios (figure 3.4 and 3.6), therefore the cutting force will be 1/10 of the thrust force at small depth of cuts where the cutting edge radius of the tool of the same size scale to the depth of cut. This is generally not the case for depths cut much greater than the cutting edge radius, or for less negative or positive rake angle tools, where COF is greater than 1.

### 3.6.2. Thermal Effects:

The speeds for these machining processes are kept very low to minimize the effect of temperature. Speeds of 10-100 rpm were used corresponding to the X-Y axis, which are very low compared to the conventional metal machining process (such as 1000 rpm) so that the thermal effects are insignificant with the slow speeds used in these experiments.<sup>[8]</sup>

## 3.5 Conclusion

The occurrence of high pressure phase transformations of semiconductors and ceramics is often characterized by the amorphous remnant that exists on the surface and within the chip after processing. This amorphous remnant is proposed to be a result of a back transformation from the high pressure phase to an atmospheric pressure phase due to the rapid release of the pressure in the wake of the cutting tool. The high pressure phase only exists while the pressure is applied at the tip of the tool. When the pressure is relieved, the material reverts to another phase. The rate at which the pressure is released, along with the maximum pressure imposed, can also affect the resultant back transformed phase.<sup>[4]</sup> It is believed by the author that the high pressure phase transformation in poly-

crystalline SiC may be responsible for the ductile machining behavior. Direct amorphization of SiC may also be responsible for or promote ductile machining of SiC. Ongoing investigations are being conducted to further evaluate the origin of the ductile regime machining of SiC. Ductile regime machining of polycrystalline SiC is possible at penetration depths of 10 and 25nm. This behavior has been confirmed by the analysis of the chips acquired. The observed amorphous chips substantiate the claim that the (high pressure) phase transformation has occurred for this hard-brittle ceramic material (SiC) (figure 3.9). High pressure phase transformations provide for the ductile regime machining of such nominally brittle materials, at small depths of cut, small feeds (in the present work an in-feed), and correspondingly small uncut chip thickness.<sup>[8]</sup>

## CHAPTER 4

### DETERMINATION OF DUCTILE TO BRITTLE TRANSITION DEPTH (DBT) FOR CVD COATED SILICON CARBIDE

#### 4.1. Introduction

Machining of brittle materials has reached a level where more focus is towards commercial applications. The advantages of CVD coated SiC over reaction bonded SiC were discussed in chapter 1. This chapter deals with experiments performed first to determine if a ductile regime exists, then to evaluate the ductile to brittle transition (DBT) depth of CVD coated SiC for single point diamond turning.

Two kinds of CVD coated SiC were provided from two different vendors, Poco Graphite Inc. and Coors Tek Inc. The detailed explanations of experiments have been divided into different sections corresponding to the experimental plan and materials. Two major sets of experiments were performed to determine the DBT depth. One experiment involved scratching using a diamond stylus and the second one was an inclined plane experiment in which a flat nose diamond tool was used to make a scratch. The inclined plane experiment was performed only on the Poco Graphite Inc. sample.

These experiments were executed using a Universal Multi System Tribometer (UMT) from CETR Inc. Unlike precision lathes, a tribometer is typically used for experiments concerning tribological applications. The difference between precision lathes and the tribometer is that precision lathes are displacement based machines and tribometers are load based devices. The post experimental analysis, which primarily included depth measurements of the scratch, used a white light interference microscope (Wyko RST). The data shown for x and y profiles within the Wyko image were

averaged for completely ductile scratch profiles. The DBT and the brittle fracture profiles they are not averaged as they have the presence of both ductile and brittle behavior.

A comparison was made between the resultant surface (ductile/brittle) and the force data derived from the tribometer. The speeds of the scratches were kept slow at 0.005 mm/sec to minimize thermal effects.

#### **4.2. Pre- experimentation Process**

The CVD coated SiC as received from vendors (Poco Graphite Inc and Coors Tek Inc) had a very high surface roughness as shown in Table. 4.1. Initial calculations for DBT depths for CVD SiC (ref: Appendix B) revealed the number as 40 nm. Hence scratching a rough surface to find a DBT depth of 40-50nm was difficult if not impossible for the as received sample. Secondly imaging was a problem with high surface roughness, as it is difficult to image dull surfaces under white-light microscopes, which we were using for determining the scratch depths and confirm/determine the DBT. Thus polishing of these CVD coated SiC samples was done (by RAPT Inc). The resultant surface roughness values for both samples are also shown in table 4.1.

Vendor	Original Surface Roughness in nm	Final surface Roughness after polishing in nm
Poco Graphite Inc.	1200	<100
Coors Tek Inc.	675	<10

Table 4.1. Surface roughness details of CVD coated SiC samples

### **4.3. Scratching using a 5 $\mu\text{m}$ Diamond Stylus Tip**

A 5 $\mu\text{m}$  diamond stylus was used for making scratches on the surface of CVD coated SiC. This diamond stylus was moved over a span of 5mm on the sample with continuously increasing loads using the load control mode in the UMT. The loads were varied from 1 to 10 grams for the Coors Tek sample and 10 to 25 grams for the Poco Graphite sample. The scratch on Coors Tek sample was made with the new diamond stylus, whereas the used stylus after Coors Tek scratches was tried for the Poco graphite sample.

### **4.4. Results from Scratching with 5 $\mu\text{m}$ Diamond Stylus**

#### **4.4.1. Coors Tek Sample:**

The maximum scratch depths achieved in the Coors Tek sample was around 150nm. The DBT in this range (1 to 10 grams) has not been seen for the Coors Tek material. This material does look completely ductile even at these scales. Figure 4.1 gives the Wyco image of the scratch. At a depth of 120nm this scratch is ductile and there is no sign of brittle behavior, which is a very encouraging result. The force and acoustic emission data were obtained for this scratch and used to analyze the ductile to brittle nature of the scratch. Figure 4.2 shows the force and AE data. As the scratch is completely ductile the force plots and the AE data do not show any fluctuations, indicative of brittle fracture.

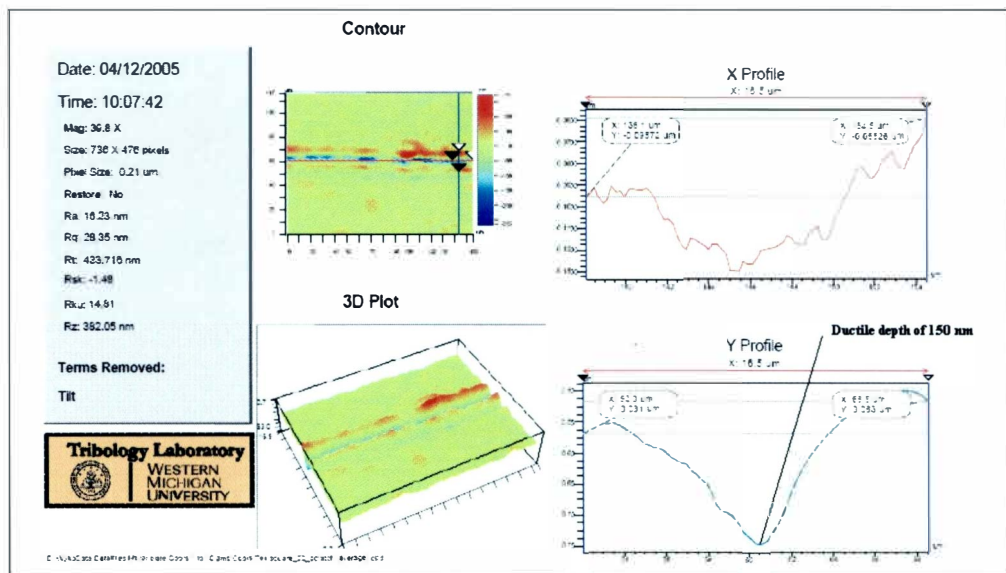


Figure 4.1: Wyko image of completely ductile scratch for Coors Tek sample using  $5\mu\text{m}$  diamond stylus

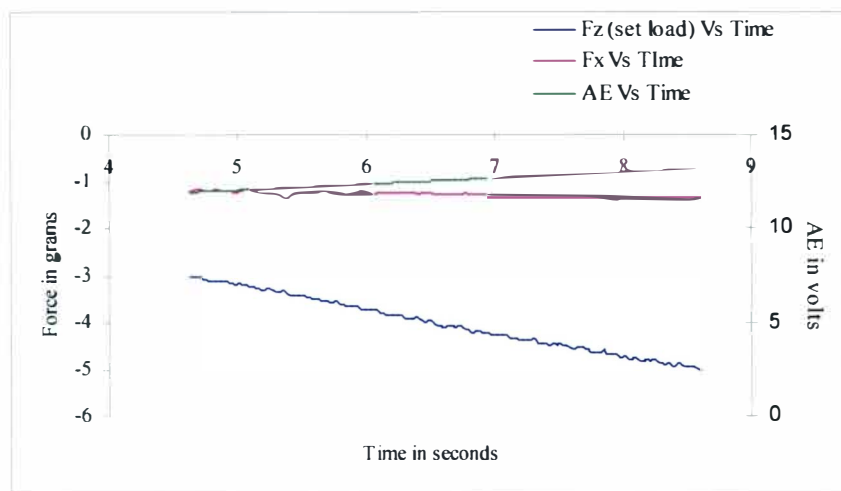


Figure 4.2: Force plot for the scratch made on Coors Tek material using  $5\mu\text{m}$  diamond stylus

#### 4.4.2. Poco Graphite Sample:

The maximum scratch depths that the Poco Graphite sample achieved were 700nm, which can be seen in figure 4.3. It is revealed from the peaks seen in the X-profile of the Wyko images that depths beyond this would be brittle, as the material is seen moving out of the surface.

There are two areas on the surface of a sample where ductile to brittle transition can take place. One is in front of the tool (at lower depths) and one is behind the tool (at higher depths). The DBT depth shown in this sample certainly is behind the tool as the material is pushed up above the surface-in the wake of the tool.

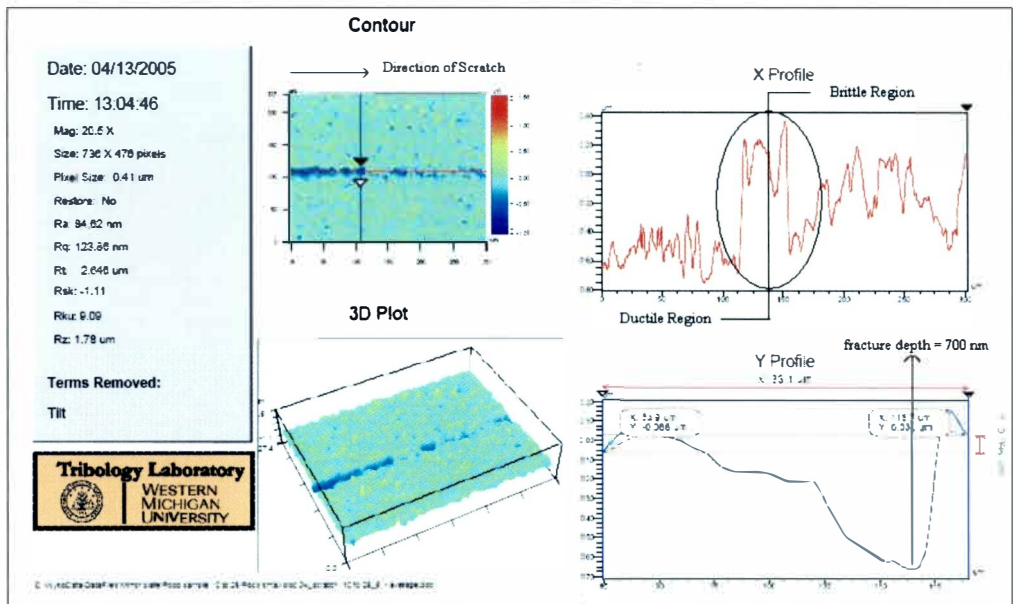


Figure 4.3: Wyko image showing DBT depth behind the tool for Poco Graphite sample using 5μm diamond stylus

The huge peak (encircled region) seen in the X-profile of figure 4.3 suggest the occurrence of brittle fracture in this region of the scratch. If the depths are ductile the scratch is formed into the surface and there is material pile up on both sides of the scratch (as shown in fig 4.1) unlike brittle fracture where the material moves above the surface of the sample unevenly.

The forces (normal and tangential) were also measured along with the acoustic emission data using the UMT. These data are shown as below in figure 4.4. The AE sensor was mounted on the tool holder away from the contact point of the diamond stylus and the surface of the sample. Hence it was difficult for the AE sensor to pick up signals from the brittle fracture. The forces shown are not for the entire scratch. The force plot



exactly corresponds to the region of the scratch shown in figure 4.3. It is difficult to determine any difference in force values as the brittle fracture occurred behind the tool. Typically fracture behind the tool is not seen in the force plots, as it is outside the sensor's measurement loop. To measure the force impulse from a major fracture event behind the tool usually requires additional sensitivity.

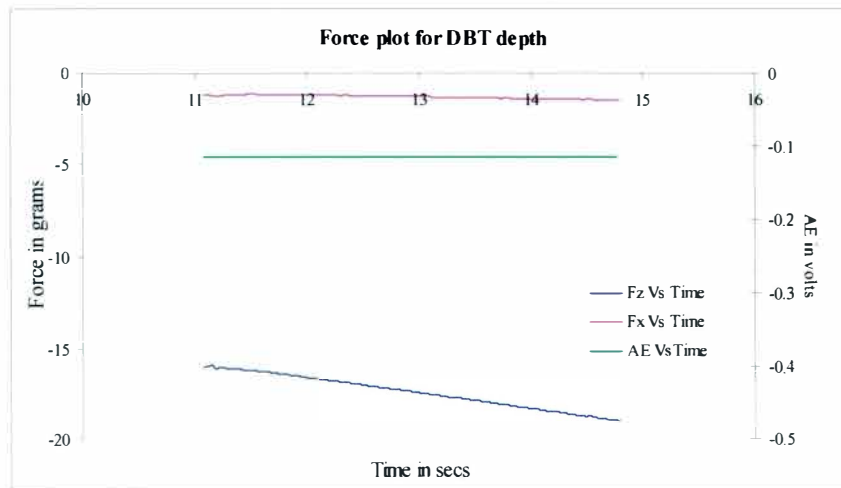


Figure 4.4: Force and acoustic emission (AE) data for Poco Graphite sample

Further experiments were performed to determine the DBT depths (in the wake of the tool). The Poco Graphite sample, which was rougher than the Coors Tek sample after polishing, was sent back for repolishing to get the surface roughness down to <10nm. The DBT for the Coors Tek sample is deeper (> 120 nm) than the calculated DBT depth (50 nm).

#### 4.5. Inclined Plate Experiment

The Poco Graphite CVD coated SiC was used for this experiment. The sample was repolished to a surface roughness of less than 10nm. These experiments were being performed to determine the DBT depths so that this information could be used for the

final goal of diamond turning CVD coated SiC. The diamond tool geometry used for the inclined plate experiment more closely represents single point diamond turning (SPDT).

A flat nose diamond tool was used for this experiment. The tool used has a -45 degree rake angle and a 5 degree clearance angle. The Poco Graphite CVD coated SiC sample was placed on an X-Y tilt stage as shown in fig. 4.5. The stage was tilted by 5 degrees, relative to the cutting edge (straight edge) of the tool, and one corner of the flat nose single crystal diamond tool makes contact with the workpiece and scratches/cuts the sample as shown in (figure 4.6). Generally a round nose tool is used for such a test, but the idea was to go deep (and produce a wide cut) into the material for determining the ductile to brittle transition depths using relatively low loads. As the corner of a flat nose tool (in  $\mu\text{m}$ ) is sharper than the edge of a round nose tool (in mm), larger depths could be obtained at lower forces.

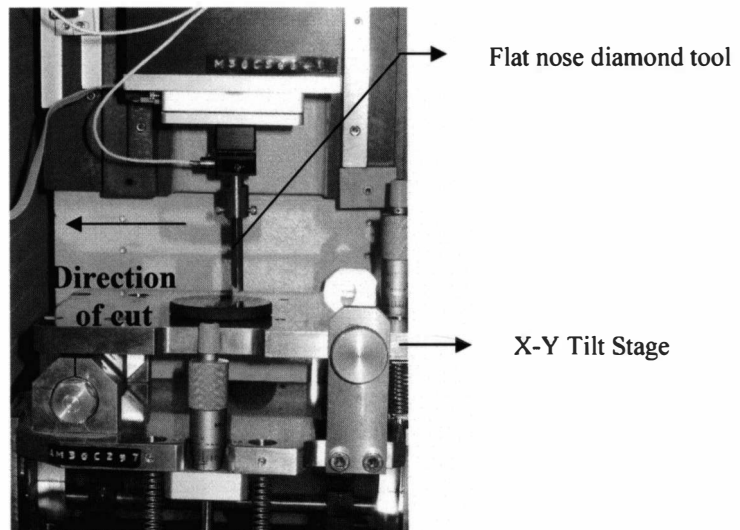


Figure 4.5: Experimental setup for inclined plate experiment

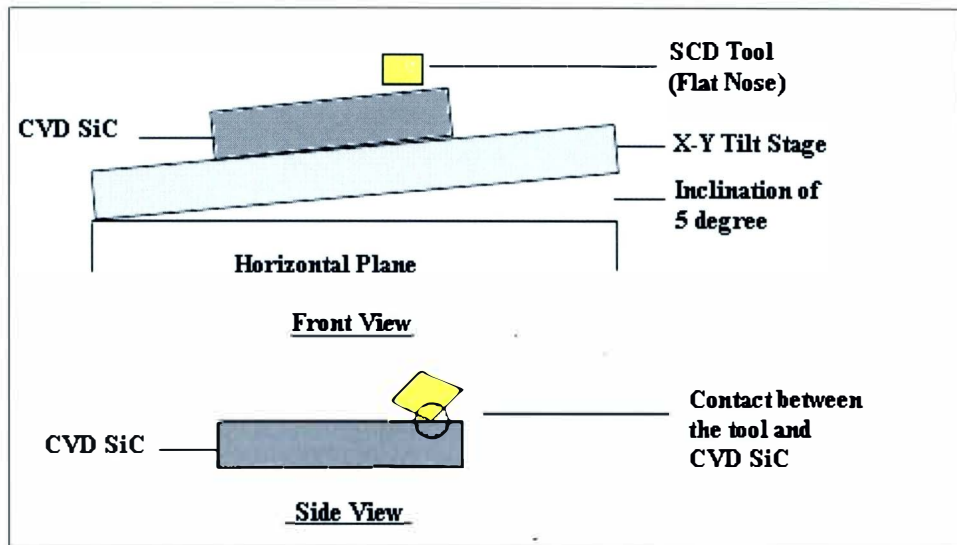


Figure 4.6: Schematic representation of the inclined plane experiment geometry

The load range used for the experiment was from 1 to 10 grams. This range was chosen as the edge of the diamond tool is much sharper than the diamond stylus, which was used previously at a higher load range (10-25 grams). Secondly the expectation for the DBT depths were in the range 40-50nm (as calculated), which are much shallower than the depths achieved previously with the diamond stylus for the higher load range of 10 to 25 gms.

#### 4.6. Results from Inclined Plate Experiment

The scratch, for the purpose of better analysis, was divided into parts. The maximum ductile depth achieved was 40 nm before the edge of the flat nose tool failed (figure 4.23). The flat nose tool was analyzed after the experiment using a scanning electron microscope. Figure 4.7 shows a part of the scratch after which the tool edge failed (40nm depth). The corresponding force plot is shown in figure 4.8.

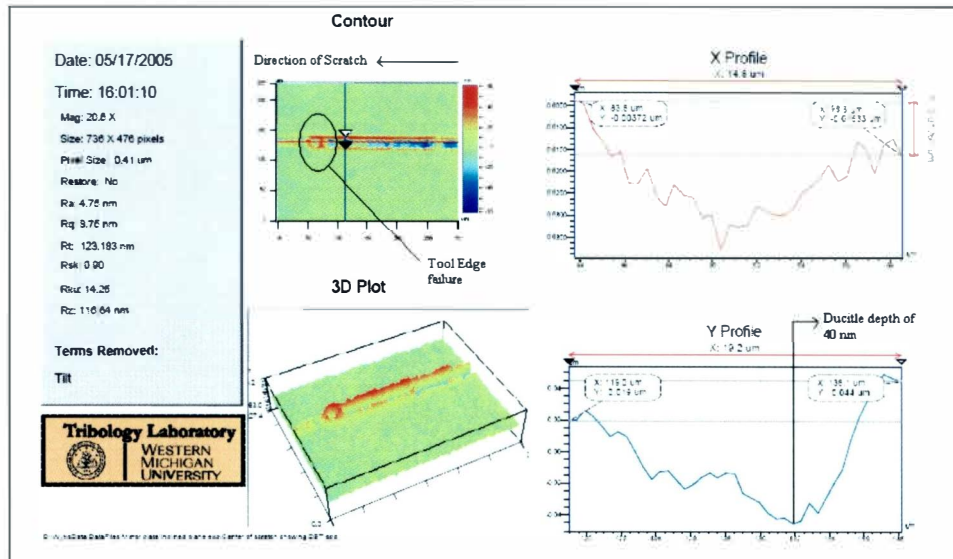


Figure 4.7: Wyko image of the DBT depth for Poco Graphite material using flat nose diamond tool

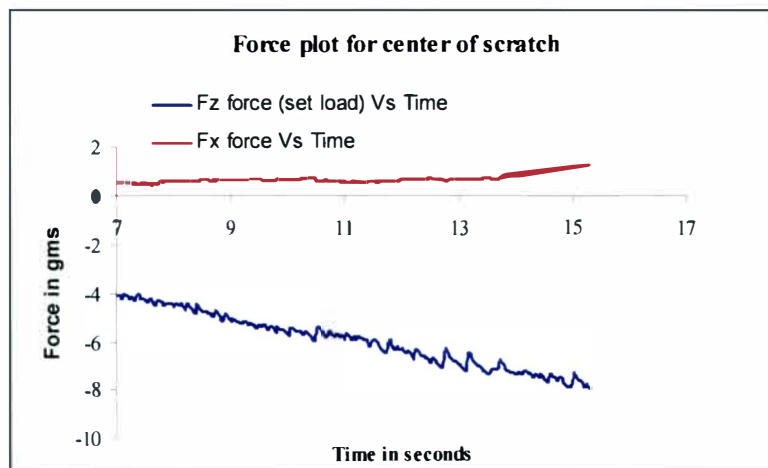


Figure 4.8: Force plot for center of scratch showing DBT for Poco Graphite material using a flat nose diamond tool

## 4.7. Scratching of using 12.5 $\mu\text{m}$ Diamond Stylus

### 4.7.1. Coors Tek Sample:

The earlier discussed Coors Tek sample scratch was ductile at depths of 120nm, to determine the DBT depth deeper scratches with higher loads were needed. Hence the scratching experiment performed earlier with a 5 $\mu\text{m}$  diamond stylus was revisited. A larger tip of 12.5 $\mu\text{m}$  tip radius was used this time (the smaller tip of radius 5 $\mu\text{m}$  was

already used for experiments so the tip was worn (broken) and not reusable, refer to figure 4.22), which also provides more deformation and larger forces, both of which enhance the sensitivity of the measurement and subsequent analysis. Since the larger tip was being used the load range for the scratch was increased to 80 - 120 gms. As the Coors Tek material was ductile even at 120nm, a deeper scratch was needed to go beyond those depths to capture the DBT.

#### 4.7.2. Poco Graphite Sample:

The maximum ductile depth achieved using the inclined plate experiment was 40 nm for the Poco Graphite sample polished for a surface roughness of less than 10 nm (Ra) and a brittle fracture behind the 5 $\mu$ m tip stylus was seen at 700 nm for the Poco Graphite sample polished for a surface roughness of less than 100nm (Ra). Thus the DBT depth was likely to be within 40-700 nm for the Poco Graphite sample. Hence to determine the actual DBT depth the scratching experiment for Poco Graphite sample was revisited. The 12.5  $\mu$ m diamond stylus was used as the smaller tip 5 $\mu$ m diamond stylus and the flat nose tool edge both had already been used. So the tools were already worn, rather broken, refer (figure 4.22 and 4.23). For this experiment a load range of 80-120 grams, same as used for the Coors Tek material. Since both of the materials were of the same type hence both were expected to have similar DBT depths, i.e. around 400 nm.

### **4.8. Results from Scratching using 12.5 $\mu$ m Diamond Stylus**

#### 4.8.1. Coors Tek Sample:

The scratch was divided into three major parts, one is the ductile region (figure 4.9 and 4.10), the second is the DBT region, and the third is the brittle region after the transition occurred (figure 4.13). Figure 4.11 shows the Wyko image of the DBT region



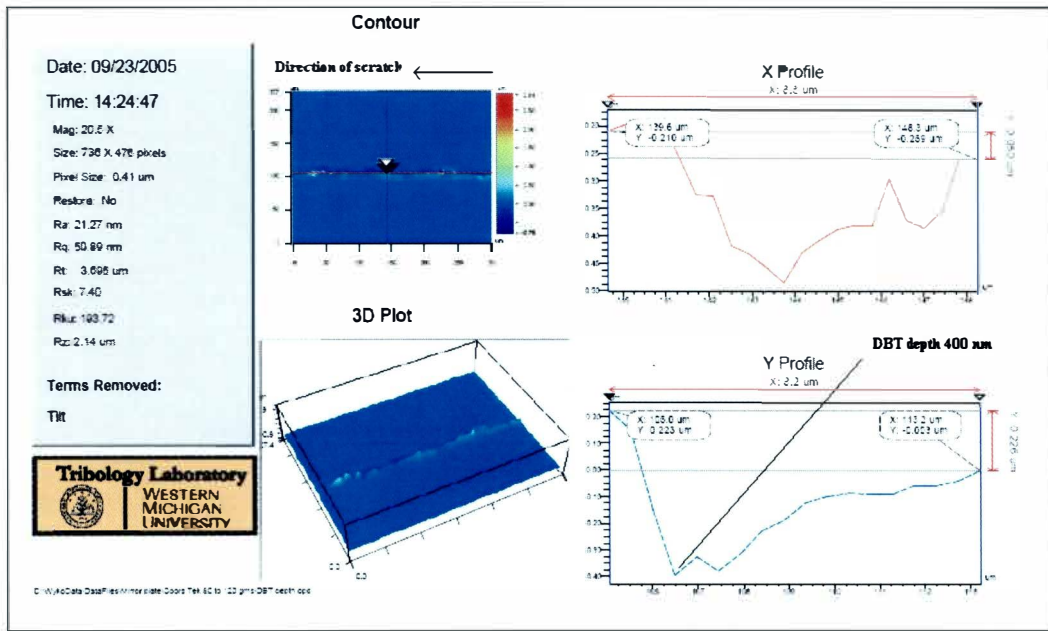


Figure 4.11: Wyko image of the DBT depth for Coors Tek sample using 12.5µm stylus

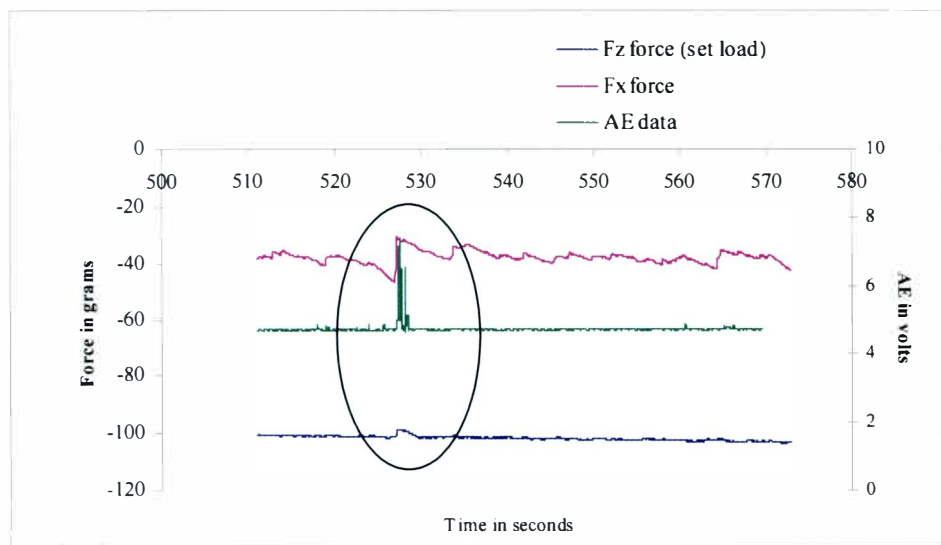


Figure 4.12: Force profile for DBT depth of Coors Tek sample using 12.5µm stylus

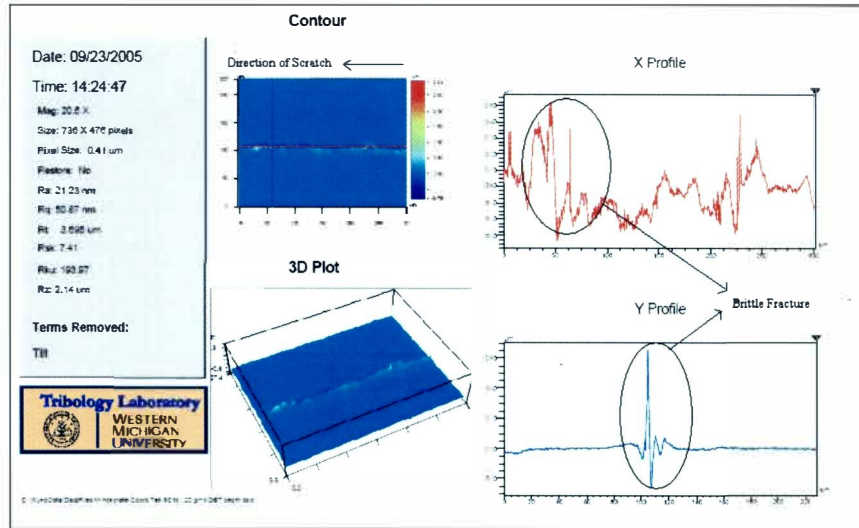


Figure 4.13. Wyko image showing the brittle fracture region after DBT depth for Coors Tek sample using 12.5μm stylus

Figure 4.13 shows the brittle fracture region after the DBT depth for the Coors Tek sample. The material moves out of the surface indicative of brittle behavior.

#### 4.8.2. Poco Graphite Sample:

The scratch was divided into three major parts, one is the ductile region (figure 4.14), the second is the DBT region (figure 4.16), and the third is the brittle region after the transition occurred (figure 4.18). The post experimental analysis for determining the scratch depths were done using Wyko, RST. The force and the AE plots follow the corresponding Wyko images (figures 4.15 and 4.17). The DBT depth was found to be 550 nm (figure 4.16).

Figure 4.17 shows the force and AE plot for DBT depth of Poco graphite sample. The encircled region is where the AE plot shows a rise and the force values go down, as it requires less energy to remove brittle material. The scratch beyond this depth was completely brittle which is shown in figure 4.18.



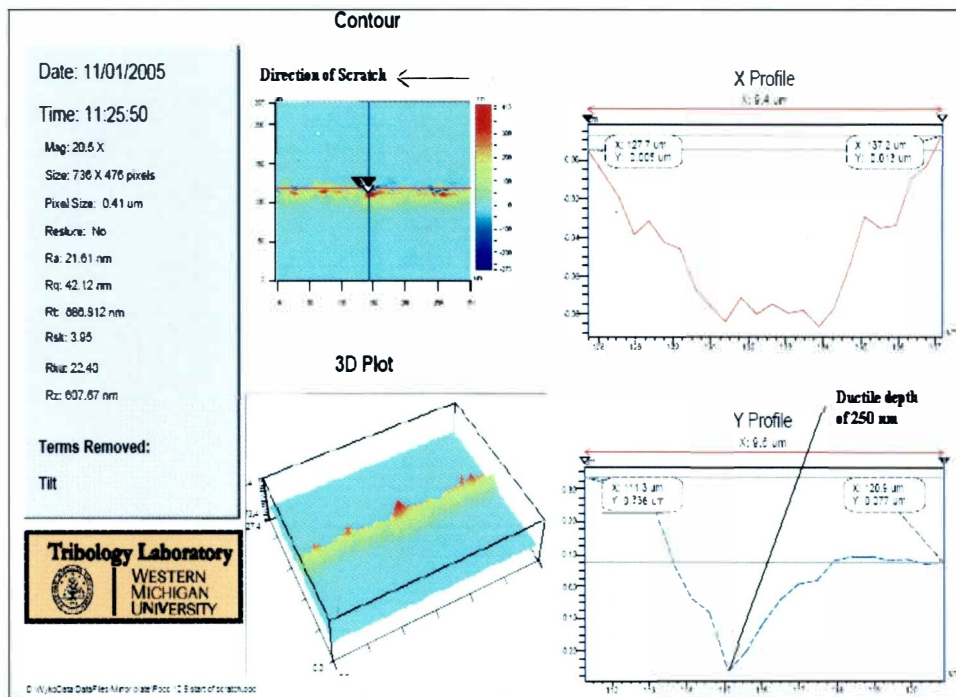


Figure 4.14: Wyko image of the starting portion of the scratch on Poco Graphite sample using 12.5 μm diamond stylus

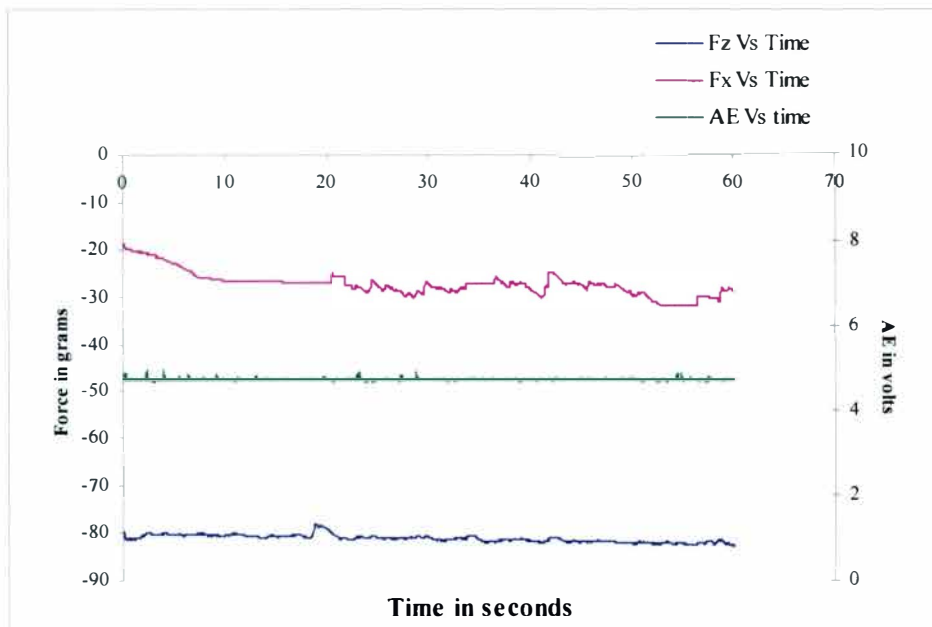


Figure 4.15: Force and AE plot for starting portion of the scratch on Poco Graphite sample using 12.5 μm diamond stylus

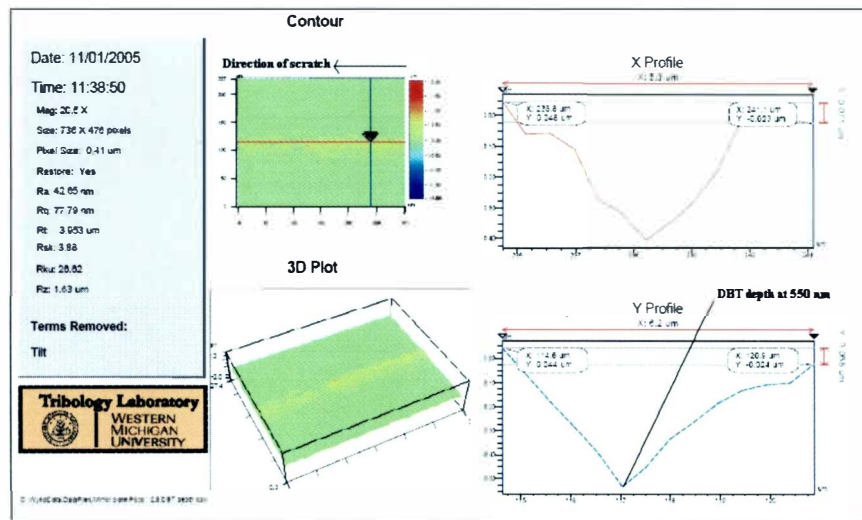


Figure 4.16: Wyko image of DBT depth for Poco Graphite sample scratched using 12.5 μm diamond stylus

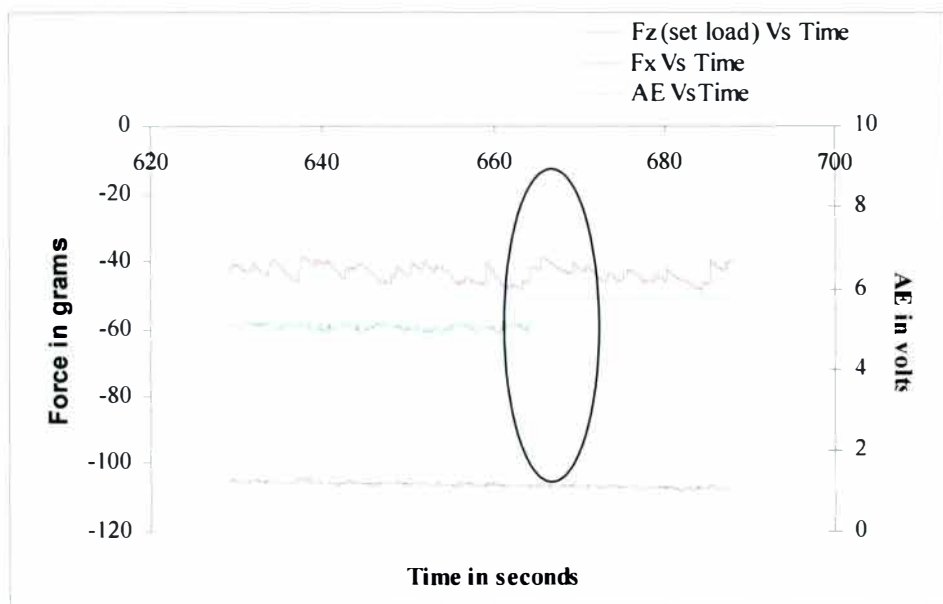


Figure 4.17: Force and AE plot of DBT depth for Poco Graphite sample using 12.5 μm diamond stylus

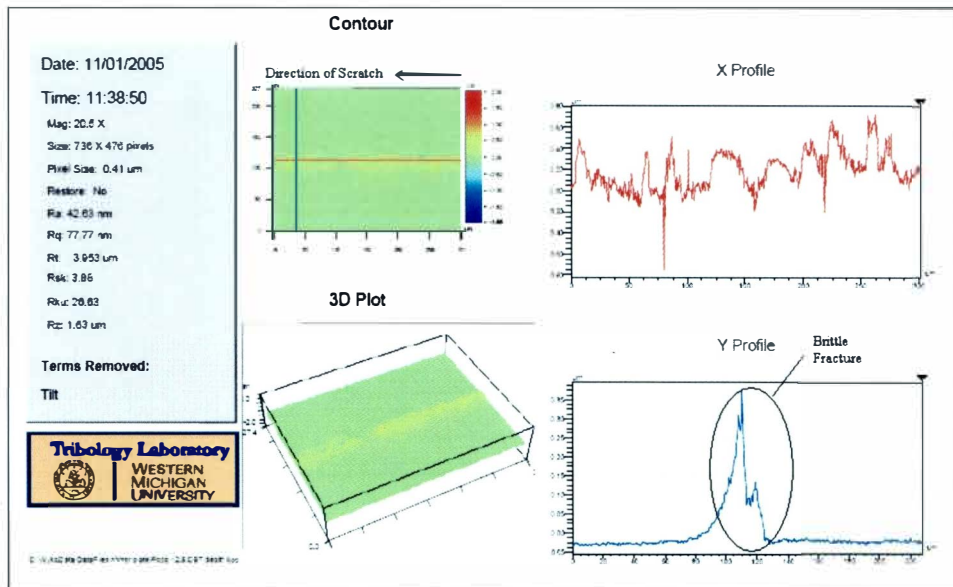


Figure 4.18: Wyko image showing the brittle fracture after the DBT region on Poco Graphite sample using 12.5  $\mu\text{m}$  diamond stylus

Figure 4.19 shows an optical image of the ductile to brittle transition for Poco graphite sample.

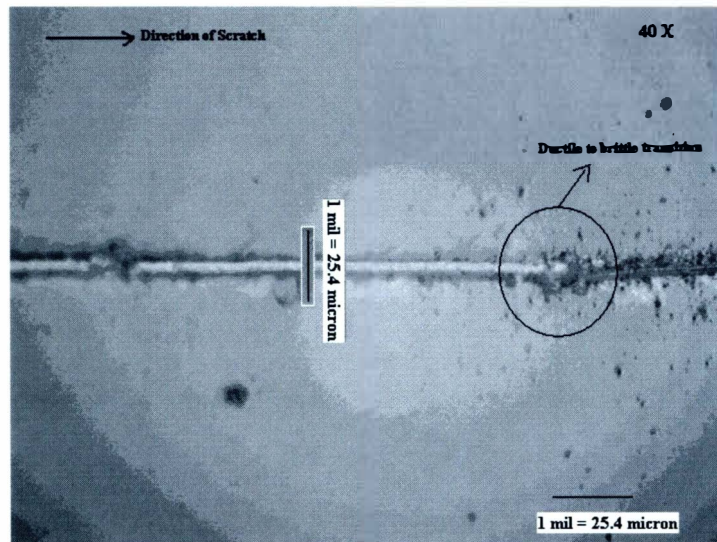


Figure 4.19: Optical image showing ductile to brittle transition of the Poco Graphite sample using 12.5  $\mu\text{m}$  diamond stylus

#### 4.9. Coefficient of Friction

The coefficient of friction data was derived from the UMT, based upon the programmed load ( $F_z$ ) and the measured friction force ( $F_x$ ). Figure 4.20 shows the coefficient of friction data for the Poco Graphite sample derived from the scratching experiments using a  $5\mu\text{m}$  diamond stylus at a load range of 10-25 gms. Figure 4.21 shows the coefficient of friction data for the Coors Tek sample derived from the scratching experiments using a  $12.5\mu\text{m}$  diamond stylus at a load range of 80-120 gms.

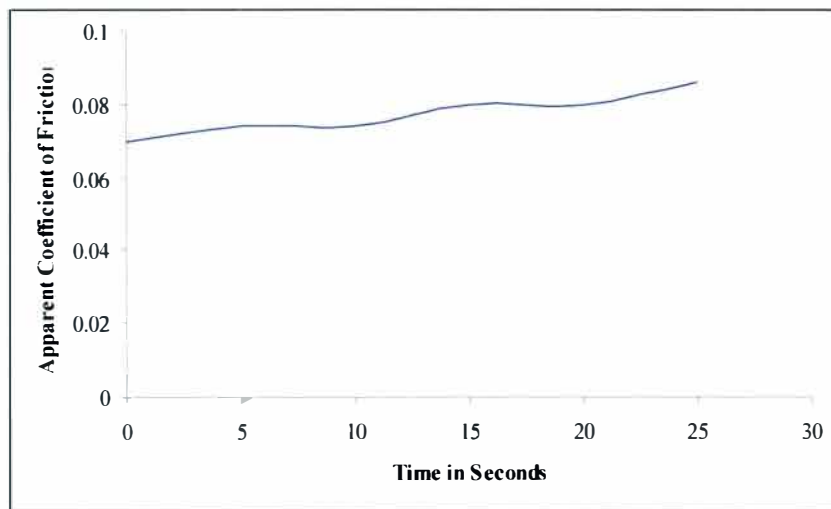


Figure 4.20: Apparent Coefficient of friction for Poco Graphite sample polished at less than 100 nm ( $R_a$ ) from scratching experiment using  $5\mu\text{m}$  stylus

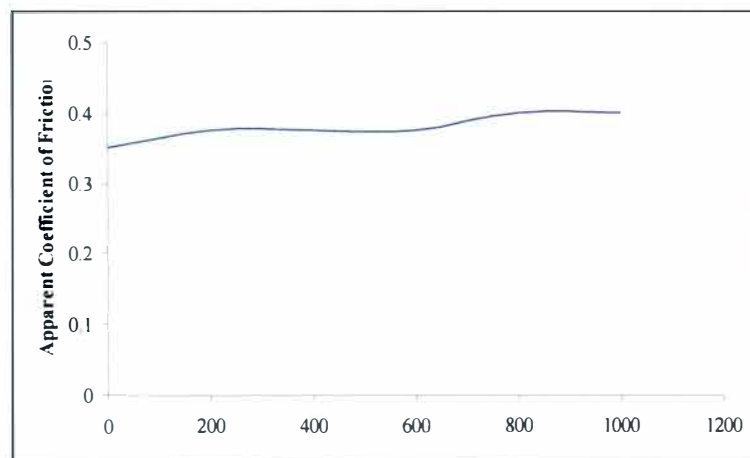


Figure 4.21: Apparent Coefficient of friction for Coors Tek sample polished at less than 10 nm ( $R_a$ ) from scratching experiment using  $12.5\mu\text{m}$  stylus

The average for friction coefficient of Poco Graphite CVD SiC was 0.08 and for the Coors Tek CVD SiC is 0.375. The coefficient of friction range for the Poco Graphite CVD SiC matches up with our expected value from previous work. The coefficient of friction value for the Coors Tek sample is higher than expected, but the scratch was done with a larger tip (12.5  $\mu\text{m}$ ) and for higher loads (80-120 grams), which may be one of the reasons for higher friction coefficient values. Secondly the Coors Tek samples underwent the process of grinding after deposition of CVD SiC on the SiC substrate, which results in a highly flat sample but the surface was not as smooth as the Poco Graphite sample (which was not ground after CVD SiC deposition).

#### **4.10. Tool Degradation**

Post experimental analysis was done for the diamond stylus used for scratching CVD SiC. Fig 4.22, 4.23 and 4.24 show images taken in a SEM for the 5  $\mu\text{m}$ , the edge of flat nose tool used for inclined plane experiment on Poco graphite sample, and the 12.5  $\mu\text{m}$  tip radii tools. The 5  $\mu\text{m}$  tip and the corner of the flat nose tool show wear on their tip (actually the tip and the edge has been broken off) as these were used for multiple scratches. The 5  $\mu\text{m}$  tips are sharper than the 12.5  $\mu\text{m}$  tips, and hence more susceptible to wear and failure. Therefore the sharper tip increases the chances of failure due to breakage. The 12.5  $\mu\text{m}$  tip was used for only two scratches and no major wear on its tip is indicated, aside from a small flat on the tip, which may have been present in the new tip.

The contact between two relatively hard materials used in all of these experiments (diamond against SiC) creates tool wear. As we try to machine or scratch SiC we also simultaneously grind diamond throughout the process (however not so obvious with the 12.5  $\mu\text{m}$  tip).

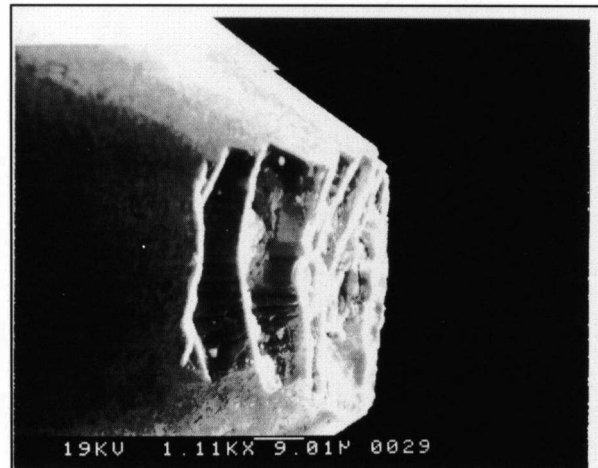


Figure 4.22: SEM image of a 5 $\mu$ m worn/broken diamond stylus tip

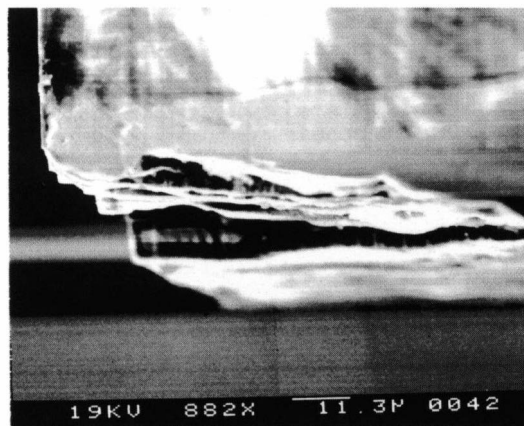


Figure 4.23: SEM image of the tool edge corner from flat nose tool used for inclined plane experiment of Poco Graphite sample

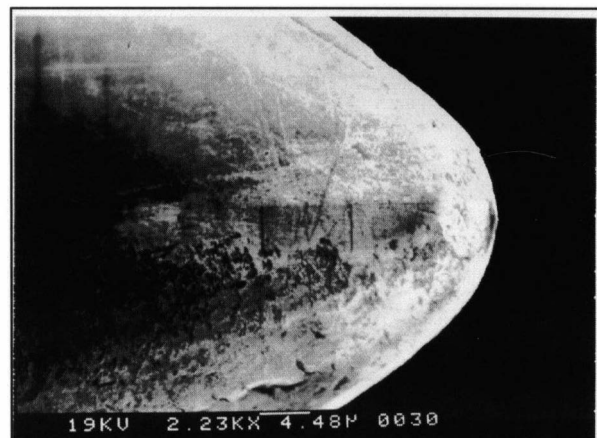


Figure 4.24: SEM image of a 12.5  $\mu$ m tip radius diamond stylus

#### **4.11. Discussion**

The DBT depth for the Poco Graphite sample was found to be 550 nm and, the DBT depth for the Coors Tek material was determined to be 400 nm. The DBT depth achieved for samples from Coors Tek and Poco Graphite sample were thus comparable. The calculated depth for the DBT (40 nm, refer: appendix B) did not match up with either of the samples. The difference in actual and calculated DBT depth might have to do with the fact that the grains in CVD coated SiC are grown in a particular direction. They most likely have directional properties similar to single crystal SiC which might be a reason CVD SiC to be ductile at 400 nm. The results of the scratching experiments were validated by calculating the imprinted image of the stylus radius using the achieved scratch depth and width (appendix E). The calculated radius did match up well with the actual stylus radius. The force plots were primarily used to deduce the DBT depths and COF.

#### **4.12. Conclusion**

Scratching has proved to be a useful experimental basis for understanding qualitatively and quantitatively the ductile and brittle mode deformations that are encountered in machining and other processes. <sup>[16]</sup> The experiments also show the dependence of loads, surface roughness, stylus geometry, relative to the quantities that characterize a scratch (load-depth profiles and the DBT).

## CHAPTER 5

### SINGLE POINT DIAMOND TURNING (SPDT) OF CHEMICALLY VAPOR DEPOSITED (CVD) COATED SILICON CARBIDE (SiC)

#### 5.1. Introduction

CVD SiC is an excellent reflective optics material exhibiting superior polishability with low scatter, exceptional thermal and cryogenic stability and high resistance to atomic oxygen and electron beam degradation. Since optics is a high priority application for this material, the final surface roughness of CVD SiC should be less than 60 nm (RMS). This level of surface roughness is achievable by processes like polishing and lapping. The primary problem that persists with polishing or lapping is the resultant flatness of the piece. The larger the diameter of the piece the more difficult it is to maintain the flatness or shape/ form accuracy. Hence to overcome the limitations of these processes (polishing and lapping) they may be replaced by single point diamond turning (SPDT).

A detailed explanation on the determination of DBT depths for CVD SiC was discussed in Chapter 4. As mentioned in chapter 1 our project goal was to machine a 6 inch diameter CVD coated SiC disk to achieve a surface roughness of less than 65nm. Chapter 4 was our first step towards SPDT of CVD coated SiC disk. The 6 inch diameter sample was fabricated by Poco Graphite Inc. and polished by RAPT.



## **5.2. Polishing of CVD SiC**

The 6 inch Poco Graphite sample was sent to, RAPT Inc. for polishing. The surface roughness of the sample was reduced from 700nm to less than 10nm (Ra). The sample was polished to minimize two major difficulties. First, to reduce tool wear, as significant tool wear was expected while machining larger samples. Secondly, to reduce the machining time, as machining a polished surface would not require more than one pass to achieve the required surface roughness and demonstrate the feasibility of ductile regime machining of CVD SiC using SPDT.

## **5.3. Machining Parameters**

The speed for machining or the cutting speed was kept slow at 0.001 mm/sec (60 rpm). The reasons for keeping the speed slow were:

- To avoid any thermal effects created at the contact point of the tool and CVD SiC
- As the UMT has a flexure design for the tool holders, at higher speeds the flexure is not stiff enough to sustain the forces generated during machining, therefore requiring slow speeds to avoid dynamic effects such as chatter.

The CVD SiC was mounted on a rotary spindle, which has a maximum speed of 5000 rpm. Trial experiments on single point turning of aluminum were performed to measure the limitations of the UMT. The experiments revealed that the UMT was stable at lower spindle speeds, usable speeds being less than 100 rpm.

As the UMT being a load/force based machine, to achieve the required depth of cut, calculations were done (ref: appendix C) to predict the weight or load that should be programmed to achieve the desired depth of cut. Chapter 4 did reveal the DBT transition depth for Poco Graphite CVD SiC as 550 nm. Since the UMT's performance was limited

to low speeds for stable operation as a cutting machine (note this is not the machine's intended use), selecting small feeds would increase the speed of the rotary drive. Hence to keep the speeds low and also have ductile cuts the final feed was selected to be  $1\text{ }\mu\text{m/rev}$ , the estimated depth  $500\text{ nm}$ , the spindle speed as  $60\text{ rpm}$  and a cutting speed of  $0.24\text{ mm/sec}$ .

#### 5.4. Experimental Setup for SPDT of CVD SiC

SPDT of CVD SiC was done using the UMT. A  $500\text{ gram}$  load cell was used for the experiment. A single crystal diamond tool was used for this experiment (ref: appendix F, fig. F2). The nose radius for the tool was  $3\text{ mm}$ , rake angle of  $-45\text{ deg}$  and a clearance angle of  $5\text{ deg}$ . Chemical mechanical polishing (CMP) slurry was used as the coolant supplied by, Buehler Inc. (Master Polish 2 ,40-6376-032) Figure 5.1 below shows the experimental set up for SPDT of CVD SiC.

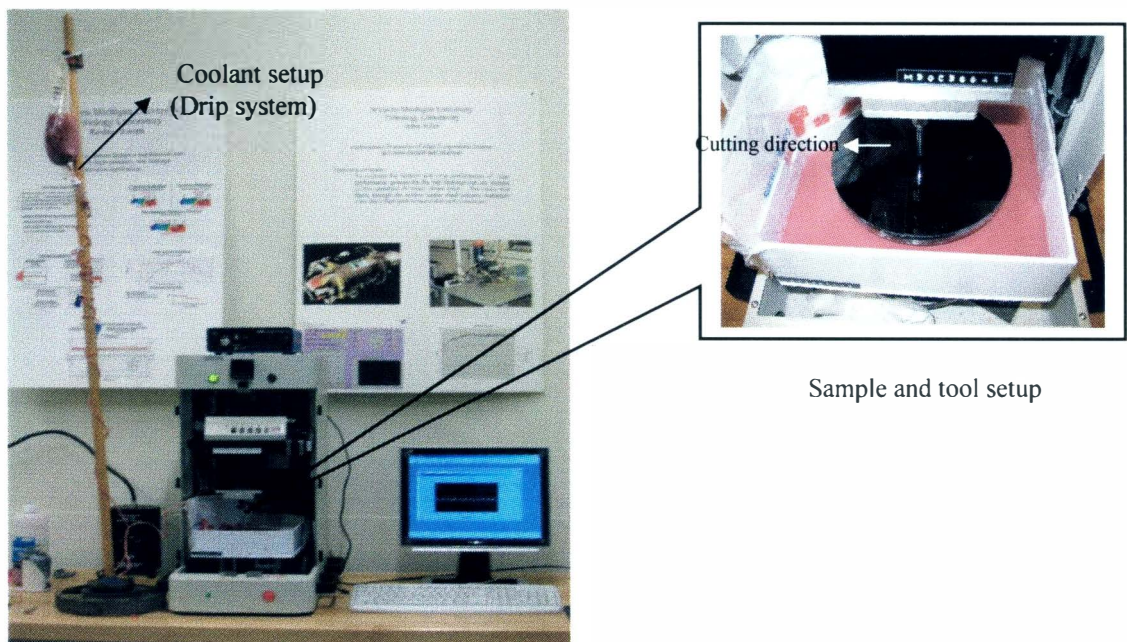


Figure 5.1: Experimental setup for SPDT of CVD SiC

The cutting direction was fixed from the center (inside) to outside. The coolant was deposited over the surface of CVD SiC sample using a drip system (similar to a thin film spin coating system).

## **5.5. Results**

### **5.5.1. Machining Time:**

The total machining time was 21 hours resulting from the fact that the feed speed was slow 0.001 mm/sec (1  $\mu\text{m}/\text{rev}$  at 60 rpm), and the part was 6" in diameter.

### **5.5.2. Surface Roughness:**

The surface roughness values were measured after machining using a Wyco RST - white light interference microscope. Figure 5.2 below shows the mirror finish achieved after machining the CVD coated SiC. Post experimental analysis of surface roughness values using the Wyco, RST is as shown as a CAD drawing in figure 5.3. The reason for having more than one region of machined surface over the 6 inch CVD SiC plate was due to the defects in the manufacturing of the coolant container (not leak proof). This resulted in dripping of the coolant into the rotary stage motor assembly leading to clogging of the spindle, and eventually causing the spindle to fail. Figure 5.4 shows images of the machined surface taken from an optical microscope at a magnification of 40X.

Wyko RST images, shown in figure 5.5 do compare well with the machining results, showing uniform feed marks for region 2 and a rougher surface (not as uniform) in region 1. The unmachined region is also shown for comparison of the surface before and after machining. In the final product or application, the feed marks (region 1 and 2) would be removed by a finish polishing operation to remove the fine surface structure generated during SPDT.

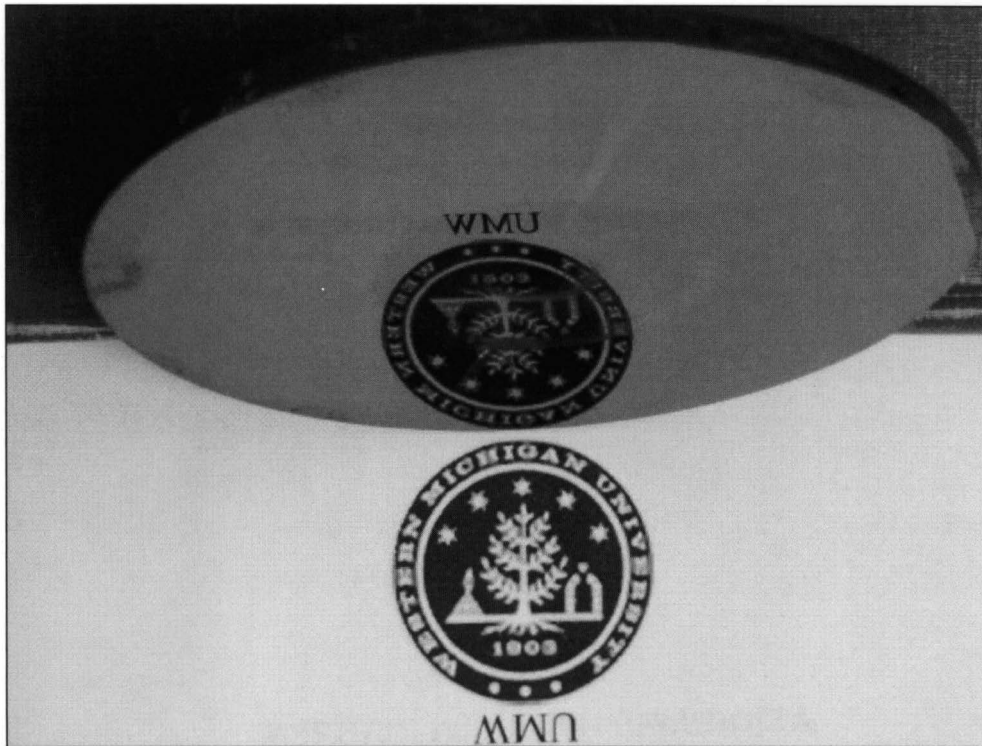


Figure.5.2: Picture showing the optical quality of the surface finish on the machined CVD SiC sample

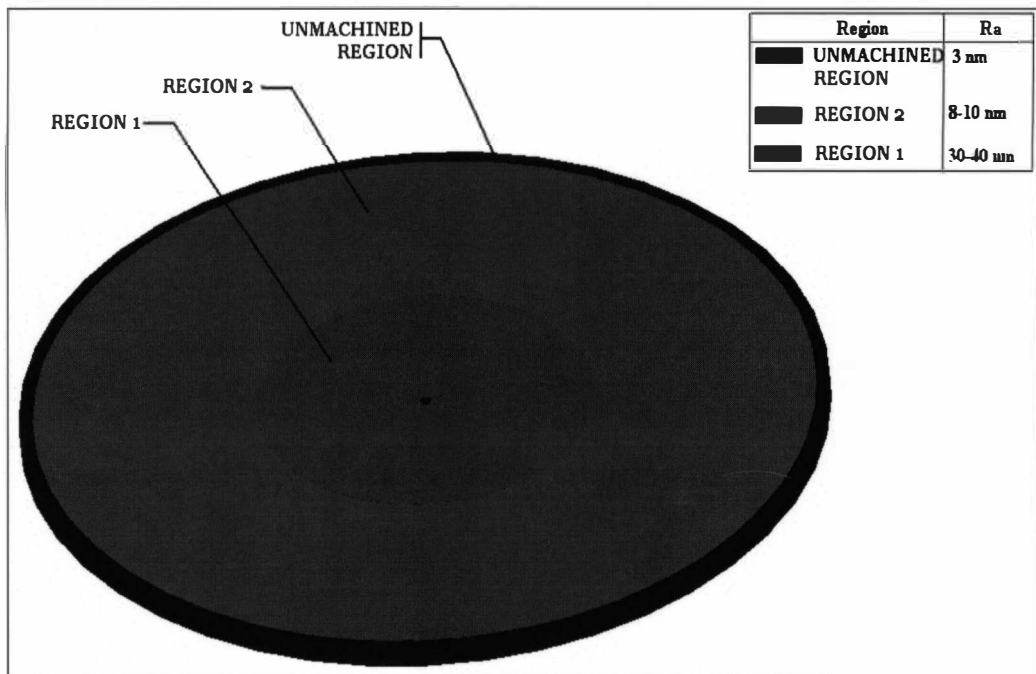


Figure 5.3: CAD model showing the surface roughness distribution for 6 inch CVD SiC plate


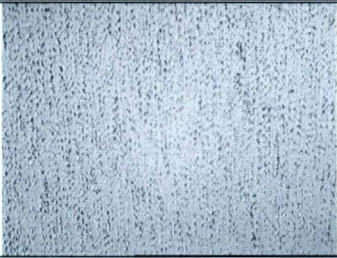

Optical Images	Regions on 6 inch sample	Surface Roughness (Ra)
	Unmachined Region	3nm
	Region 1	20nm
	Region 2	8 -10nm

Figure 5.4: Optical images comparing CAD drawing

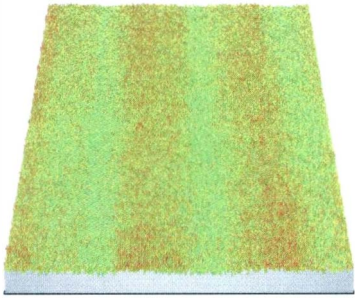
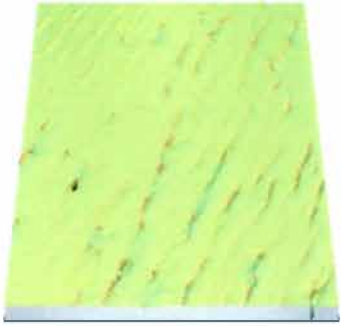
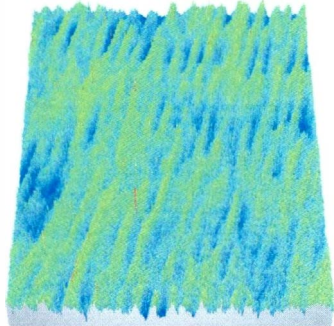
		
Unmachined Region	Region 1 Surface Roughness 30-40 nm	Region 2 Surface Roughness 8-10nm

Figure 5.5: Wyko images comparing the surfaces before and after machining

### 5.5.3. Tool Wear:

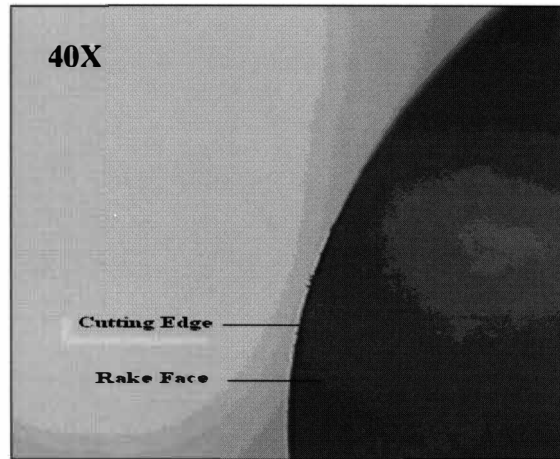


Figure 5.6: Optical microscope image of tool edge after machining

Figure 5.6 shows optical image of the tool edge used for SPDT of CVD SiC. There is no chipping or fracture on the cutting edge of the tool. Due to minimal wear at the tool edge the tool can be resharpened and used again for future experiments. Hence the usage of CMP slurry as the cutting fluid did seem to enhance the tool life to a great extent.

### 5.5.4. Depth of Cut:

Table 5.1 below shows the difference between programmed and actual depth of cut from machining.

Region	Programmed Depth of cut	Actual Depth of cut
Region 1	500 nm	350 nm
Region 2	500 nm	200 nm

Table 5.1: Comparison of programmed and achieved depth of cuts

The UMT used for SPDT of CVD SiC is a load/force based machine and it has a flexure design for the tool/stylus holders. The flexure results in deflection in the sensitive direction (in-feed or depth) compared to a DTM, which are generally displacement based



controlled. As mentioned above the spindle failed at one point of time (end of region 1) during machining due to clogging of the coolant, this resulted in demounting the tool and the sample and then cleaning the complete motor assembly to make it workable again. The difference in depth of cut between region 1 and 2 might be due to remounting of the tool (machining in region 2), which may not have been mounted properly earlier (machining in region 1) as seen from the surface profile and the non uniform feed marks on region 1 (figure 5.5) i.e. if tool fixtures are not properly mounted the machined surface are expected to deteriorate as the tool used is not properly oriented and loose. Also calculations of the depth of cut were only estimates and did not include the effect of the cutting edge radius. At this time these effects have not been analyzed to the fullest, work is being done to resolve these problems.

Figure 5.7 below compares the actual measured depth of cuts with the surface roughness values. Region 2 with a smaller depth of cut produced the better surface finish as would be expected. Region 1 with higher depth of cuts produced high surface roughness values.

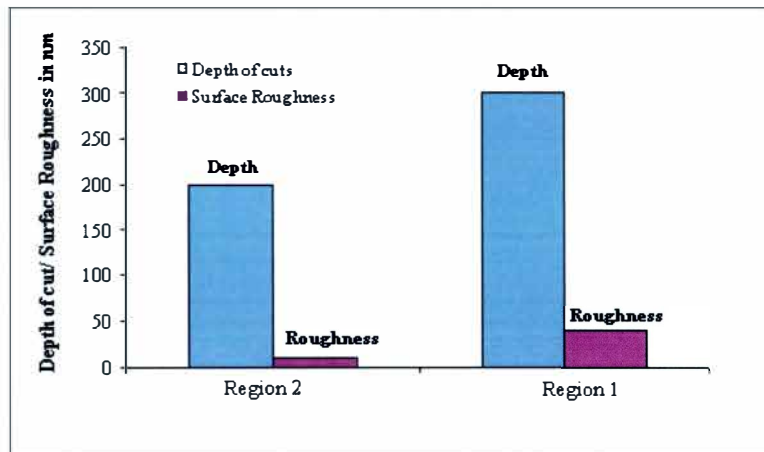


Figure 5.7: Comparison of depth and surface roughness data

#### 5.5.5. Feed/ Rev:

The programmed feed/rev was  $1\text{ }\mu\text{m}/\text{rev}$ . Figure 5.8 below shows the actual feed/rev from machining in region 2 (figure 5.5), taken using an optical microscope. The scale on the image confirms that the actual feed/rev after machining was the same as the programmed feed i.e. there are 10 feed/marks per  $10\text{ }\mu\text{m}$  distance.

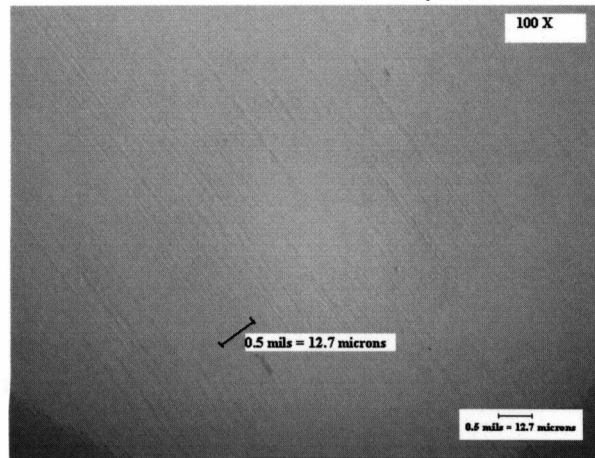


Figure 5.8: Optical image of the machined surface showing the actual feed/rev for region 1

#### 5.5.6. Material Removal:

Figure 5.9 below shows a schematic explaining the step height difference between the machined and the unmachined regions. The calculated volume of total material removed was  $2.996\text{ mm}^3$  (ref: Appendix D). The respective volume of material removed was  $0.696\text{ mm}^3$  from region 1 and  $2.3\text{ mm}^3$  from region 2.

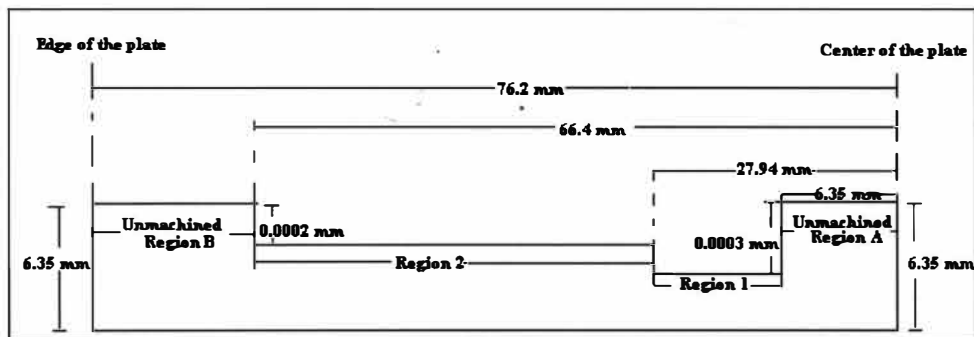


Figure 5.9: Schematic showing a sectional view of the 6 inch plate comparing the step size for depth of cuts



## **5.6. Discussion**

The surface roughness of less than 20 nm was achieved on the 6 inch CVD coated SiC disk. The machining speed was kept slow to nullify thermal effects between the tool and the material. Enhanced methods of coolant supply will be adopted in future experiments to avoid problems related to leakage of the coolant. Tool wear analysis was not an objective of this study; hence detailed tool wear analysis will be reported in future work. The material removal calculations do suggest that the use of coolant has helped sustaining the cutting edge of the tool when good volume of material has been removed.

## **5.7. Conclusion**

Ductile Regime SPDT of CVD SiC was possible, achieving the required surface roughness value of less than 65 nm. Further optimization of the process parameters are required for enhanced machining of CVD SiC. The potential replacement of intermediate processes like grinding, polishing and lapping, by SPDT, would reduce the total manufacturing cost by increasing productivity and improving surface form accuracy.

## **5.8. Ongoing Work on SPDT of CVD SiC**

Presently work is being done on SPDT of unpolished CVD coated SiC sample from Poco Graphite Inc. and a laser machined sample from Mount Laser Inc. The chart below shows the number of passes made on the surface and the corresponding surface roughness achieved after each pass. The machining parameters used for SPDT of these samples are exactly the same discussed above for the 6 inch Poco Graphite sample.

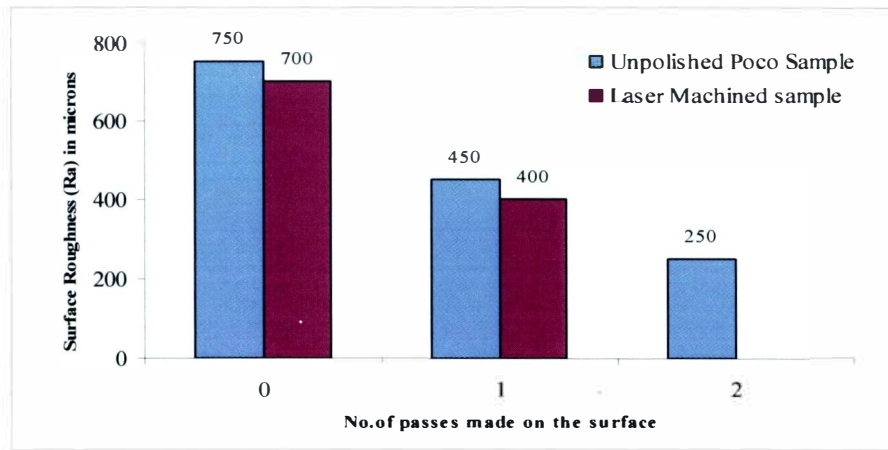


Figure 5.10: Chart showing the surface roughness achieved for different samples after each pass of machining

The programmed depths of cut for the samples are 500 nm but the actual depths are 200-300 nm similar to that seen in the 6 inch sample. More details regarding the SPDT of these samples would be reported in future work.

## CHAPTER 6

### DETERMINATION OF A DUCTILE RESPONSE AND A DUCTILE TO BRITTLE TRANSITION DEPTH OF QUARTZ (Infrasil 302)

#### 6.1. Introduction

Heraeus Inc. INFRASIL 302 is an optical quartz glass grade manufactured by fusion of natural quartz crystals in an electrically heated furnace. It combines excellent physical properties with outstanding optical characteristics, especially in the IR and the visible wavelength range. The index homogeneity is generally controlled and specified in either one direction (the direction of use or functional direction) or multiple dimensions.

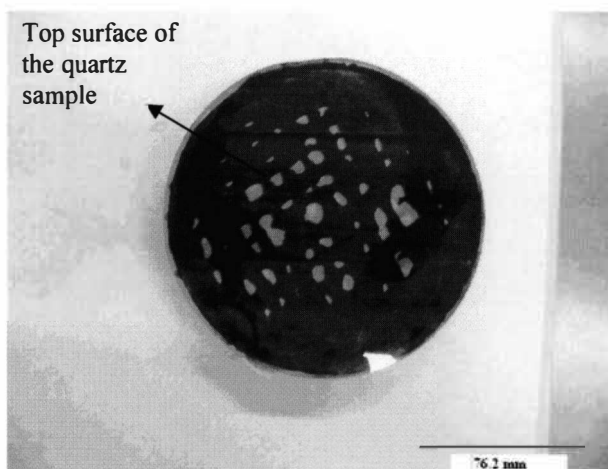


Figure 6.1. Picture showing the Quartz (Infrasil 302) used for scratches

Scratching experiments were performed on Infrasil 302 (figure 6.1) to determine if a ductile response was possible and then to further determine the ductile to brittle transition depth (DBT), i.e. critical depth of cut or penetration. Scratches were made by moving a diamond stylus or a single crystal diamond flat nose tool over a polished Infrasil 302 surface, RAPT Inc. had previously polished the surface to a roughness of less than 10nm rms. During the scratching operation the horizontal forces and the acoustic emission signals were recorded. In post experimental analysis the depth and width of the

scratch was measured using a white light interference microscope (Wyko, RST). The data for depth and width of scratch retrieved from Wyko was averaged for ductile scratches. The Wyko images showing DBT transition depths were not averaged as they included both ductile and brittle depths. These experiments were divided into two major types. The first type involved scratching using a 5  $\mu\text{m}$  diamond stylus tip, and the second type used an inclined plate experiment with a flat nose single crystal diamond tool. All scratches were made at slow speeds of 0.001 mm/sec (1  $\mu\text{m}/\text{sec}$ ), to avoid any thermal effects. The experimental set up for the scratching of Infrasil 302 using the 5  $\mu\text{m}$  diamond stylus was exactly the same as discussed in chapter 4 for CVD SiC. In this chapter the results for the scratch tests and the DBT depths are presented and discussed.

## **6.2. Scratching of Quartz with a 5 $\mu\text{m}$ Diamond Stylus**

The scratch was done with a load range of 20 to 50 grams. At about 22 grams the scratch had a catastrophic fracture, indicating a DBT depth at 120nm, which can be seen in the Wyko image (figure 6.2) below. The force plots also show a reduction in the force values and the AE shows a peak at about 22 grams indicating brittle fracture. The DBT occurred at the initial part of the scratch, brittle behavior was seen throughout the scratch after the DBT depths (figure 6.4). The fall in the force values and the rise in acoustic emission data as shown in figure 6.3 suggest the occurrence of a DBT.

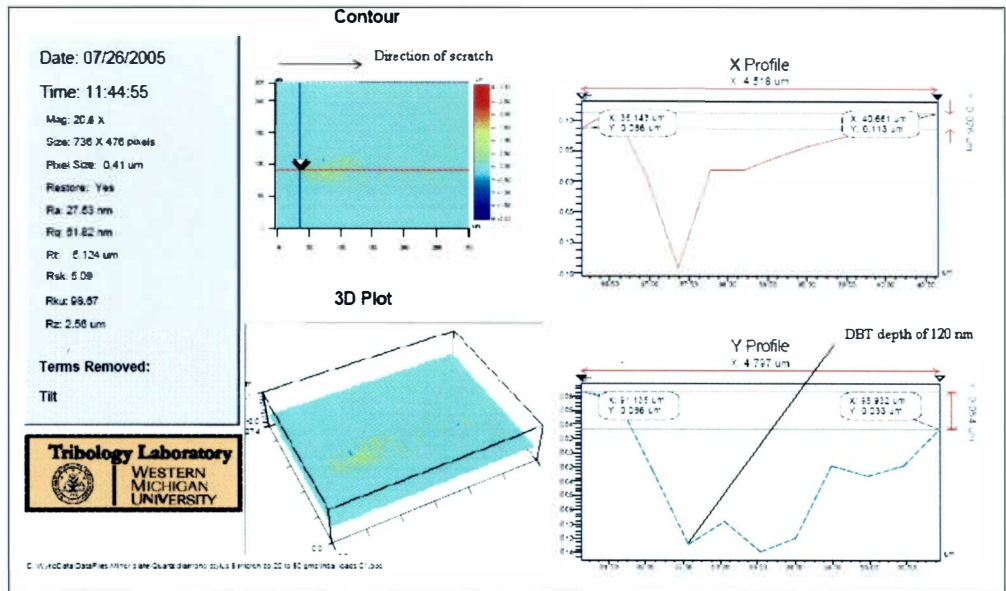


Figure 6.2. Wyko image for the scratch showing the DBT depth of Infrasil 302 using 5µm stylus

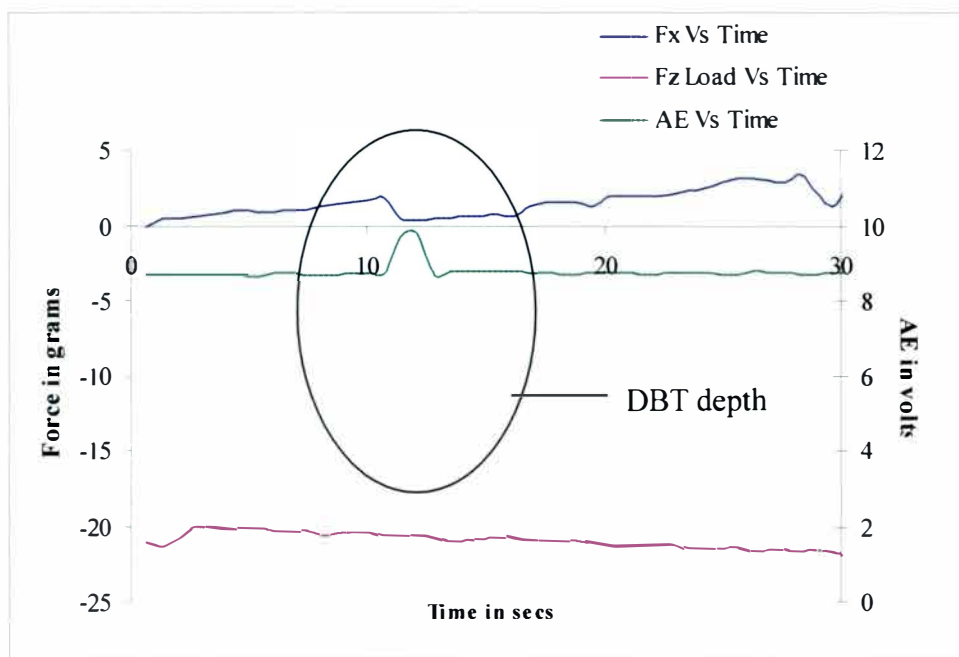


Figure 6.3. Force plot for the scratch showing the DBT depth of Infrasil 302 using 5µm stylus

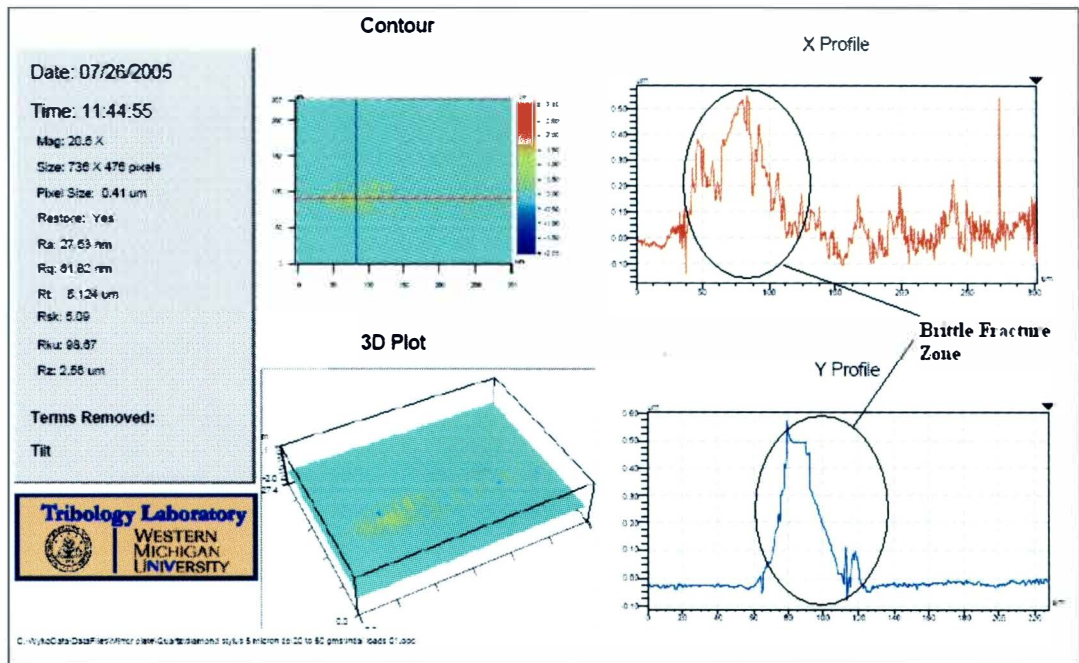


Figure 6.4: Wyko image showing the brittle fracture zone after the DBT depth of Infrasil 302 using 5 μm stylus

### 6.3. Inclined Plate Experiment

#### 6.3.1. Experimental Setup for Inclined Plate Experiment:

The same Quartz piece (Infrasil 302) as used above was also used for this experiment. A flat nose diamond tool was used for this experiment. The tool has a -45 degree rake angle and a 5 degree clearance angle. The quartz sample was placed on an X-Y tilt stage as shown in figure 6.5. The stage was tilted by 10 degrees, relative to the cutting edge (straight edge) of the tool, and one corner of the flat nose single crystal diamond tool makes contact with the work-piece and scratches/cuts the sample (figure 6.11). The scratch was done for a load range of 20 to 50 grams, as the DBT depth was found in the same load range for the scratch made using 5 μm diamond stylus.

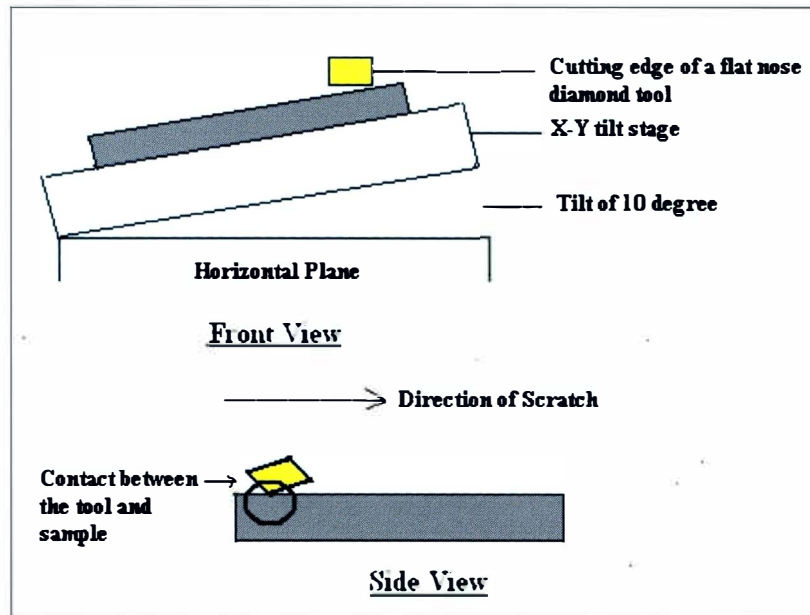


Figure 6.5. Schematic representation of the experimental set up for inclined plate experiment

### 6.3.2. Results from Inclined Plate Experiment:

Figures 6.6 and 6.7 show the DBT depth revealed from the inclined plate experiment to be approximately 120 nm. Beyond this depth material was ejected up from the surface rather than making a scratch (indent or penetration) into the surface, indicating brittle behavior (figure 6.8). The force plots show a fall in the force values and the AE shows a peak at about 24 grams indicating brittle fracture.

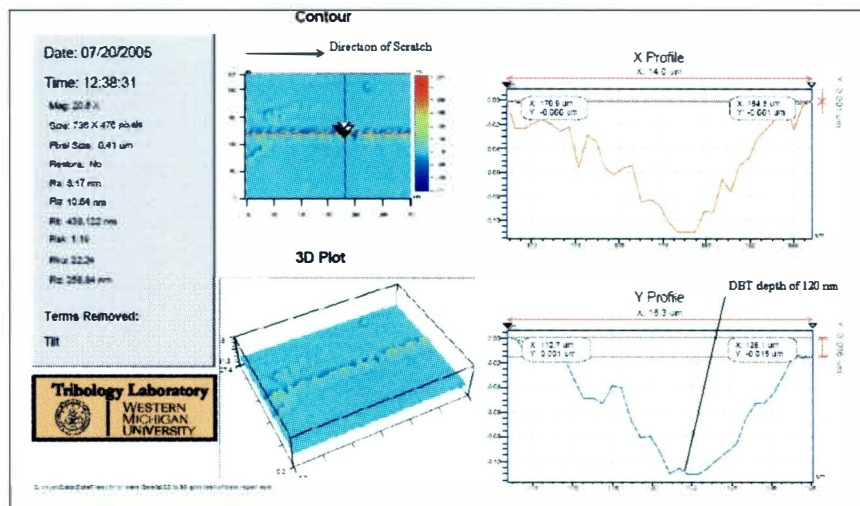


Figure 6.6. Wyco image showing DBT depth for scratch on Infrasil 302 from inclined plate experiment

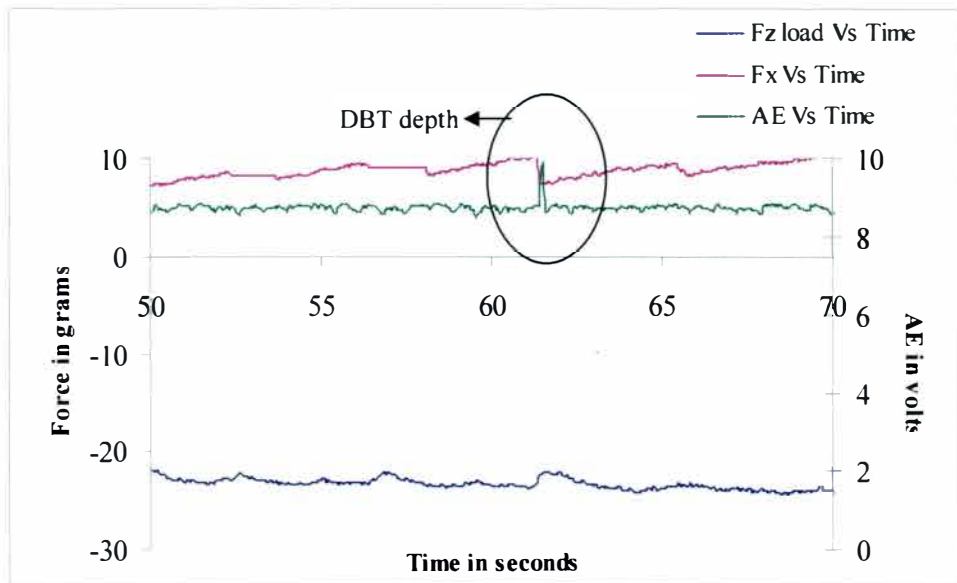


Figure 6.7. Force plot for DBT depth of scratch on Infrasil 302 from inclined plate experiment

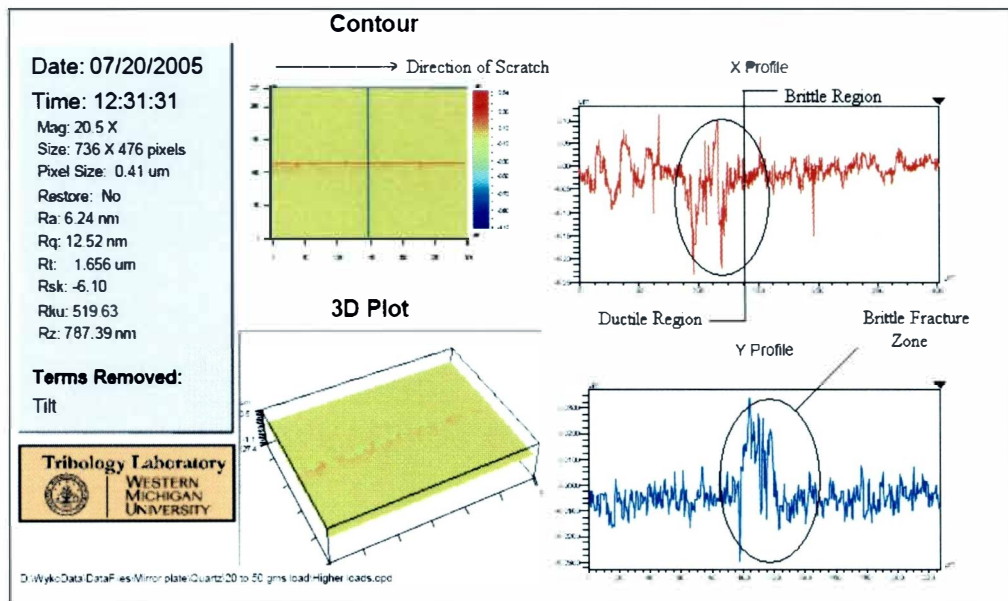


Figure 6.8. Wyko image showing the brittle region of the scratch on Infrasil 302 from inclined plate experiment



## 6.4. Discussion

A brittle mode and a DBT (critical depth of 120 nm) for the material were seen within the load range of 22-24 grams for the scratches made by both the diamond stylus and the inclined plate experiment (using the flat tool). This work suggests a DBT depth for quartz at 120 nm for both the scratch made using a diamond stylus and for the scratch from the inclined plate experiment. Table 6.1 below summarizes the experiments conducted to determine the DBT depths of quartz.

Experiment type	Tool used	Loads used in grams	Depth of scratch or DBT depth in nm	Nature of scratch
Scratching	5 micron diamond stylus	10 to 20	100	Ductile
Scratching	5 micron diamond stylus	20 to 50	120	DBT depth @ 22 grams
Inclined plate	Flat nose tool, -45° chamfer	20 to 50	120	DBT depth @24 grams

Table 6.1. Summary of experiments performed to determine DBT in quartz

## 6.5. Conclusion

The existence of ductile regime in quartz (Infrasil 302) was determined performing different scratching experiments. The DBT depth determined from experiments at 120 nm is comparable to the calculated DBT critical depth of 180nm (ref: appendix B). The results of the scratching experiments were validated by calculating the imprinted image of the stylus radius using the achieved scratch depth and width (appendix E). The calculated radius did match up well with the actual stylus radius. The force plots were primarily used to deduce the DBT depths.

## CHAPTER 7

### CONCLUSION

#### 7.1. Concluding Remarks

The research and extensive study done on the machining of brittle materials, such as SiC in the previous chapters and by others <sup>[8,23]</sup>, does reveal the fact that these materials (semiconductors, ceramics, and optics) can be machined in the “ductile regime.” Ongoing investigations are being conducted to further evaluate the origin of the ductile regime machining of SiC <sup>[8, 24]</sup>

##### 7.1.1. Polycrystalline SiC:

Ductile regime machining of polycrystalline SiC is possible at penetration depths of 10 and 25nm. This behavior has been confirmed by the analysis of the machining chips acquired and surface roughness (chapter 3).

The ductile response of semiconductors and ceramics are often characterized by the amorphous remnant that exists on the surface and within the chip after machining <sup>[8]</sup>. The origin of this amorphous remnant is believed to be caused by the occurrence of a high pressure phase transformation <sup>[23]</sup>. It is believed, by the author and others <sup>[7,8 and 23]</sup> that the high pressure phase transformation in (poly-crystalline) SiC may be responsible for the ductile machining behavior.<sup>[8]</sup> Direct amorphization of SiC may also be responsible for or promote ductile machining of SiC <sup>[23]</sup>, as the amorphous form of ceramics are generally softer and more ductile than their crystalline counterparts. <sup>[25]</sup>

##### 7.1.2. CVD SiC:

The DBT depth or critical depth of cut or penetration depth, for the CVD coated SiC from Poco Graphite Inc. was found to be 550 nm and, the DBT depth for the CVD

coated SiC from Coors Tek Inc. was determined to be 400 nm. The DBT depths determined for Poco Graphite and Coors Tek sample were comparable, as the samples were of the same type. The experiments also show the dependence of loads, surface roughness, stylus geometry, and the quantities that characterize a scratch (load-depth profiles and the DBT) (chapter 4). The presence of a ductile mode or response in CVD SiC was proved by performing ductile scratches, and determining the DBT. This result informed the SPDT process of CVD SiC i.e. established the necessary process parameters. These process parameters (DBT depths) were used for machining of CVD SiC to achieve mirror finish surfaces (chapter 5).

#### 7.1.3. Quartz:

Chapter 6 dealt with the identification and analysis of a ductile deformation mode in quartz (Infrasil 302). The DBT transition depth was found to be 120nm for both stylus and cutting tool scratch tests. The determined DBT depth compared well with the calculated DBT depth of 180 nm (Appendix B). Scratching of quartz to determine the DBT depth was a precursor to performing ductile regime machining of quartz.

## **7.2. Future Developments**

#### 7.2.1. Polycrystalline SiC:

Efforts should be made to optimize tool wear while machining of polycrystalline SiC by using a coolant or cutting fluid. Additional experiments to determine the DBT depth for polycrystalline SiC are required.

#### 7.2.2. CVD SiC:

The author suggests measuring the tool cutting edge radius before and after machining of CVD SiC, to map the tool wear ratio. Another suggestion is to perform

similar experiments on SPDT of CVD SiC in a displacement based machine (precision lathes) where there is direct control over the depths of cut or in-feeds used for machining. The potential replacement of intermediate processes like finish grinding, polishing and lapping, by SPDT, would reduce the total manufacturing cost by increasing productivity and improving surface form accuracy.

#### 7.2.3. Quartz:

The author suggests performing SPDT of quartz and monitoring the tool wear. It would be beneficial to measure the cutting edge radius of each tool before performing each experiment.

## REFERENCES

1. [www.ceramicbulletin.org/months/Sep99/Kingery.pdf](http://www.ceramicbulletin.org/months/Sep99/Kingery.pdf)
2. [http://www.ifm.liu.se/matephys/new\\_page/research/sic/Chapter2.html](http://www.ifm.liu.se/matephys/new_page/research/sic/Chapter2.html)
3. [www.cvdmaterials.com/sicoptic.htm](http://www.cvdmaterials.com/sicoptic.htm)
4. W.S.Blackley and R.O.Scattergood, 1994, Chip topography for ductile regime machining of Germanium, Journal of Engineering for Industry, vol. 116, pp 263-266.
5. C.Morris, D.L.Callan, J.Kulik, J.A. Patten, and R.O. Scattergood, 1995, Origins of Ductile Regime in Single –Point Diamond Turning of Semiconductors, Journal of the American Ceramic Society, v78, n8, pp 2015-2020
6. T.G.Bifano, T.A.Dow, and R.O. Scattergood, 1991, Ductile Regime Grinding: A New Technology for machining brittle materials, Transactions of the ASME, 113, pp 184-189
7. Y.G. Gogotsi, A.Kailer and K.G.Nickel, 1997, Phase Transformations in Materials studied by Micro-Raman spectroscopy of Indentations, Materials Reserve Innovations, v1, pp 3-9
8. J.A. Patten, W. Gao and K.Yasuto, 2005, Ductile Regime Nanomachining of Single-Crystal Silicon Carbide, ASME, v127, pp 522- 532
9. M. Yoshida, M. Ueno, K.Takemura and O. Shimomura, 1993, Pressure Induced phase transition in SiC, The American Physical Society, v48, n14, pp 587-590
10. P.S. Pizani, R. Jasinevicius, J.G. Duduch and A.J.V. Porto, 1999, Ductile and Brittle modes in single-point-diamond-turning of silicon probed Raman scattering, Journal of Material Science Letters, v18, pp 1185-1187
11. P.N. Blake and R.O. Scattergood, 1990, Ductile-Regime Machining of Germanium and Silicon, Journal of American Ceramic Society, v73, n4, pp 949-957
12. T. Nakasuji, S.Kodera, S.Hara and H. Matsunaga, 1990, Diamond turning of Brittle Materials for Optical Components, CIRP Annals 39, 1, pp 89-92
13. Fritz Klocke, Oliver Gerent and Christoph Schippers, Green Machining of Advanced ceramics, in Machining of Ceramics and Composites, Eds Jahanmir and Said, New York Mercel Dekker Inc., 1999, pp 1-9
14. L.Yin, Eric. Y J. Vancoille, Kuppuswamy Ramesh and Han Huang, 2004, Surface Characterization of 6H-SiC (0001) substrates in indentation and abrasive

- machining, International Journal of Machine tools and Manufacture, v44, pp 607-615
15. T.Shibata, S.Fujii, E.Makino, and M.Ikeda, 1996, Ductile Regime Turning Mechanism of single crystal silicon, Precision Engineering 18, pp 129-137
  16. H.H.Hurt and D.L.Decker, 1984, Tribological Considerations of the Diamond Single-Point Tool, SPIE, v508, pp 126-131
  17. R.G. Jasinevicius, J.G. Duduch and A.J.V. Porto, 2001, Investigation on diamond Turning of Silicon crystal- Generation Mechanism of Surface cut with Worn Tool, Journal of Brazilian Society of Mechanical Sciences, v23, n2, pp 1-16
  18. A.Broese van Groenou, N.Maan and J.B.D. Veldkamp, 1979, Single point scratches as a basis for understanding grinding and Lapping, Science of Ceramic machining and Surface finishing II.
  19. Ronnie Rex Fesperman Jr., Ductile Turning of Silicon Nitride, Mechanical Engineering Masters Thesis for the University of North Carolina at Charlotte
  20. Takashi Matsumura, Takenori Ono, Kanda Nishiki-cho and Chiyoda-ku, Glass Machining with Ball and End Mill, Transactions of NAMRI/SME, v33, pp 319-326, 2005
  21. K.W.Peter, Densification and Flow phenomena of Glass in Indentation Experiments, Journal of Non-Crystalline Solids, v5, pp 103-115, 1970
  22. Y. Takeuchi, K.Sawada, T. Sata, Ultraprecision 3D Micromachining of Glass, Annals of CIRP, v45, pp 401-404, 1996
  23. John A Patten, Harish Cherukuri and Jiwang Yan, Ductile- Regime Machining of Semiconductors and Ceramics, in High – Pressure Surface Science and Engineering, Eds. Y.Gogotsi and Domnich, Institute of Physics Publishing, Bristol, U.K., pp 543-632
  24. [www.micro.physics.ncsu.edu](http://www.micro.physics.ncsu.edu)
  25. Izabela Szlufarska, Aiichiro Nakanu, Priya Vashishta, A Crossover in the Mechanical Response of Nanocrystalline Ceramics, Science, v309, pp 911-914, 2005
  26. <http://www.coorstek.com/semi.asp>
  27. <http://www.poco.com/us/SiliconCarbide/materials.asp>
  28. [www.haraeusoptics.com](http://www.haraeusoptics.com)

29. F.Z.Fang and V.C. Venkatesh, 1998, Diamond cutting of Silicon with Nanometric Finish, CIRP Annals 47, 1, pp 45-49
30. Biswarup Bhattacharya, John A. Patten, Jerry Jacob, Pater J.Blau, Jane Howe and Jason D. Braden, 2004, Ductile Regime Nano-Machining of polycrystalline Silicon Carbide, In proceedings of ASPE Annual Meeting 2004, Norfolk, VA

## APPENDIX A

### MATERIAL PROPERTIES OF POLYCRYSTALLINE SiC, CVD SiC AND QUARTZ

Common Name	CVD SiC		Poly crystal SiC	
	Value	Units	Value	Units
Young's Modulus	466.0	GPa	427.5	GPa
Poisson's Ratio	0.26	-	0.21	-
Melting Temperature	2500	$^{\circ}\text{C}$	2500	$^{\circ}\text{C}$
Thermal Conductivity	129.0	W/m.K	155.7	W/m.K
Density	3.18E3	g/cc	3.15E3	g/cc
Hardness, H	27	GPa	27	GPa
Fracture Toughness, $K_{\text{c}}$	3.3E6	$\text{Pa.m}^{0.5}$	3.5E6	$\text{Pa.m}^{0.5}$

Table A1: Material properties of polycrystalline and CVD SiC <sup>[26,27]</sup>

Common Name	Infrasil 302	
	Value	Units
Young's Modulus	70	GPa
Poisson's Ratio	0.17	-
Melting Temperature	1730	$^{\circ}\text{C}$
Thermal Conductivity	1.38	W/m.K
Density	2.203	g/cc
Hardness, H	9.8	GPa
Fracture Toughness, $K_{\text{c}}$	4E6	$\text{Pa.m}^{0.5}$

Table A2: Material properties of Infrasil 302 (quartz) <sup>[28]</sup>



## APPENDIX B

### DUCTILE TO BRITTLE TRANSITION DEPTH CALCULATIONS

#### **CVD SiC:**

Properties derived from Table A1:

Elastic modulus,  $E = 466 \text{ GPa}$

Hardness,  $H = 27 \times 10^9 \text{ Pa}$

Fracture Toughness,  $K_{IC} = 3.3 \times 10^6 \text{ Pa.m}^{0.5}$

Critical depth of cut,  $d_c = 0.15 \cdot (E/H) (K_{IC}/H)^2 [3]$

Substituting the material properties into the above equation we get

$$d_c = 38.674 \times 10^{-9} \text{ m or } 38.674 \text{ nm}$$

#### **Quartz:**

Properties derived from Table A2:

Elastic modulus,  $E = 70 \text{ GPa}$

Hardness,  $H = 9.8 \times 10^9 \text{ Pa}$

Fracture Toughness,  $K_{IC} = 4 \times 10^6 \text{ Pa.m}^{0.5}$

Critical depth of cut,  $d_c = 0.15 (E/H) (K_{IC}/H)^2 [3]$

Substituting the material properties into the above equation we get

$$d_c = 180 \times 10^{-9} \text{ m or } 180 \text{ nm}$$

## APPENDIX C

### CALCULATIONS FOR REQUIRED LOAD FOR SPDT OF CVD SiC

#### Calculation for Cutting Energy:

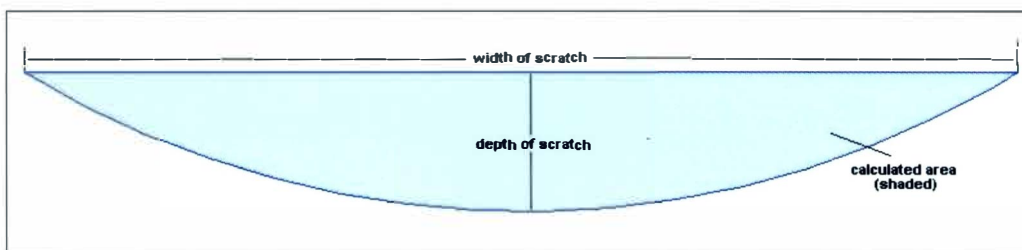


Figure C1: Schematic of the chip cross sectional area calculated for scratching experiments

Expt. type	Depth of cut in nm	Cutting force in N ( $F_x$ )	Thrust force in N ( $F_z$ )	Cross-sectional area from scratch in $\text{mm}^2$	Pressure in GPa
Scratching using $12.5 \mu\text{m}$ tip	550	0.4	1	$1.3 \times 10^{-5}$	30.769*

Table C1: Summary of inclined plate scratching experiments for Poco Graphite sample

The DBT transition depth as 550 nm (figure 4.16) for the Poco Graphite sample was determined from scratching experiments using  $12.5 \mu\text{m}$  diamond stylus (ref: chapter 4). The width and depth for the scratch was determined from figure 4.16. Figure C1 shows the schematic for profile of the scratch used to calculate the area. The area calculations were done using MATLAB program. Forces were picked from the respective force plot of the scratch (figure 4.17).

Specific cutting energy calculated from inclined plate experiment

Cross-sectional area of the chip from scratching,  $A = 1.3 \times 10^{-5} \text{ mm}^2$

Cutting force,  $F_x = 0.4 \text{ N}$

Cutting Energy,  $E_{sc} = F_x / A = 30.769 \text{ N-m/mm}^3$

\* - Comparable to recent work done on diamond anvil cell where pressure of 33 GPa was determined for phase transformation/amorphization of SiC. [Levitas, 2005]

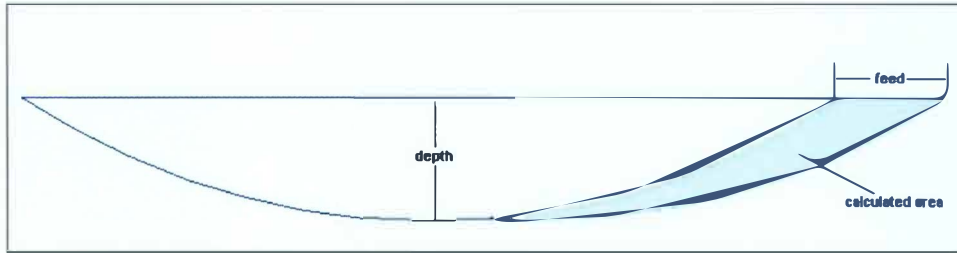


Figure C2: Schematic of the chip profile for area calculations during SPDT

Depth of cut in mm	Cross-sectional area in mm <sup>2</sup>
0.0005	$2.4898 \times 10^{-7}$

Table C2: Summary of chip area for different depths of cut

### Weight required for 500 nm depth of cut:

Chip cross-sectional area,  $A_c = 2.4898 \times 10^{-7} \text{ mm}^2$

Cutting force,  $F_x = E_{sc} \times A_c = 8.19 \times 10^{-3} \text{ N}$

COF = 0.1 (assumed from previous work)

Thrust Force,  $F_z = 8.19 \times 10^{-2} \text{ N}$

**Weight required,  $w = 8.19 \text{ grams}$**

The above derived weight was used for the programmed the load during SPDT of CVD SiC for a depth of cut 500 nm and a feed  $1 \mu\text{m/rev}$ .

## APPENDIX D

### CALCULATIONS FOR VOLUME OF MATERIAL REMOVAL AFTER SPDT of CVD SiC

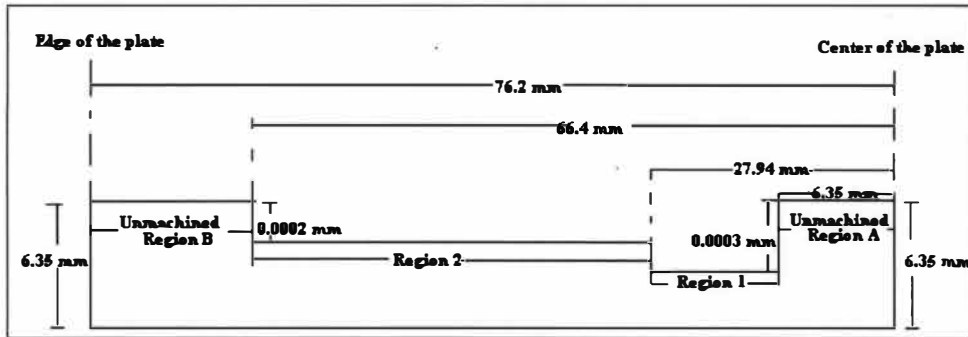


Figure 5.9: Schematic showing a sectional view of the 6 inch plate comparing the step size for depth of cuts

Volume of material removed from machining in region 1 as shown in fig.5.9:

If the material removed from region 1 with dimensions is as shown below:

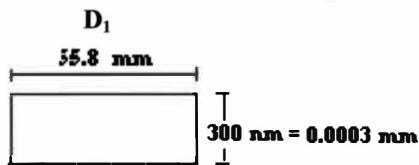


Figure D1 : Cylinder from Region 1

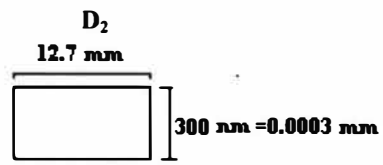


Figure D2 : Cylinder from unmachined Region A

Volume of the cylinder =  $\pi \times \text{diameter}^2 / 4 \times \text{height}$

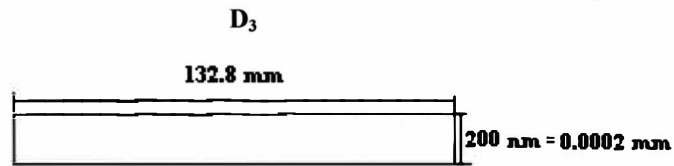
Height ( $h_1$ ) in this case is 300 nm

Volume of material removed from machining region 1 =  $\pi \times h_1 \times [(D_1^2 - D_2^2)/4]$

Therefore volume of material removed from region 1,  $V_{\text{reg1}} = 0.696 \text{ mm}^3$

Volume of material removed from machining in region 2:

If the material removed from region 2 is considered as a cylinder with dimensions as shown below:



**Figure D3 : Cylinder from Region 2**

Volume of material removed from machining region 2 =  $\{\pi \times h_2 \times [(D_3^2 - D_1^2)/4]\}$

Height ( $h_2$ ) in this case is 200 nm

Therefore volume of material removed from region 2 =  **$2.3 \text{ mm}^3$**

The total volume of material removed =  **$2.996 \text{ mm}^3$**

## APPENDIX E

### CALCULATION FOR VALIDATION OF SCRATCHING EXPERIMENTS

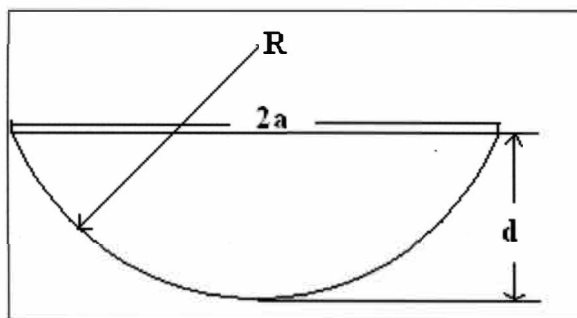


Figure E1: Schematic representation of the scratch parameters used for calculation

#### Formula used for validation:

If

$2a$  – width of the scratch

(derived from Y-profiles of Wyko image)

$R$  – radius of the tool used

$d$  – depth of the scratch

(derived from Y-profiles of Wyko image)

Then

$$R = \{(a^2/d)+d\}/2$$

Sample	Actual tool radius	Calculated tool radius
Poco Graphite	12.5 $\mu\text{m}$	11.02 $\mu\text{m}$
Coors Tek	12.5 $\mu\text{m}$	16.5 $\mu\text{m}$
Quartz	5 $\mu\text{m}$	6.34 $\mu\text{m}$

Table E1: Comparison of the calculated and the actual tool radius

## APPENDIX F

### DIAMOND CUTTING TOOL DESIGNS USED FOR DIFFERENT EXPERIMENTS

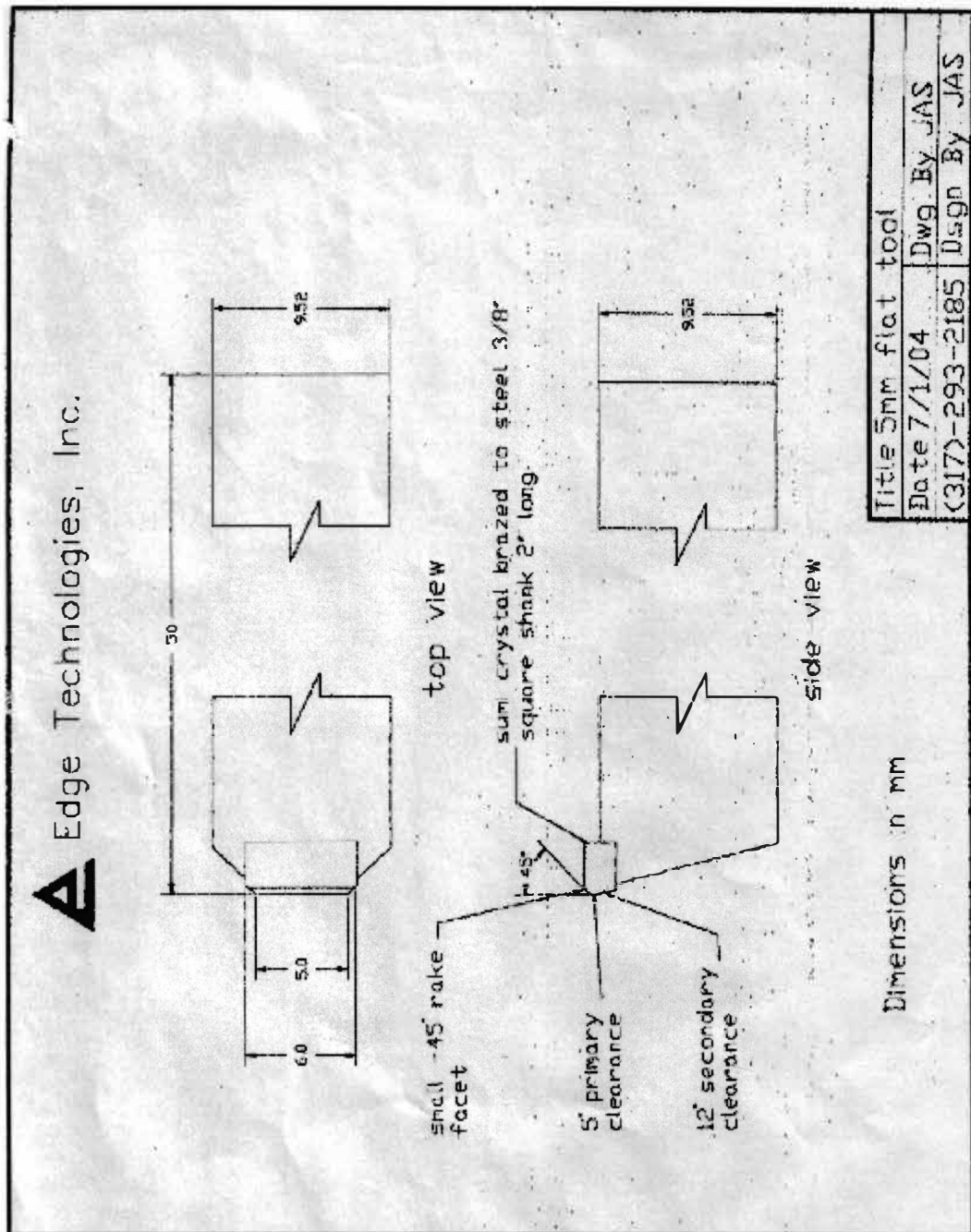


Figure F1: Design of a Flat nose single crystal diamond tool with  $-45$  degree chamfer used for DTM of polycrystalline SiC

## Chardon Tool

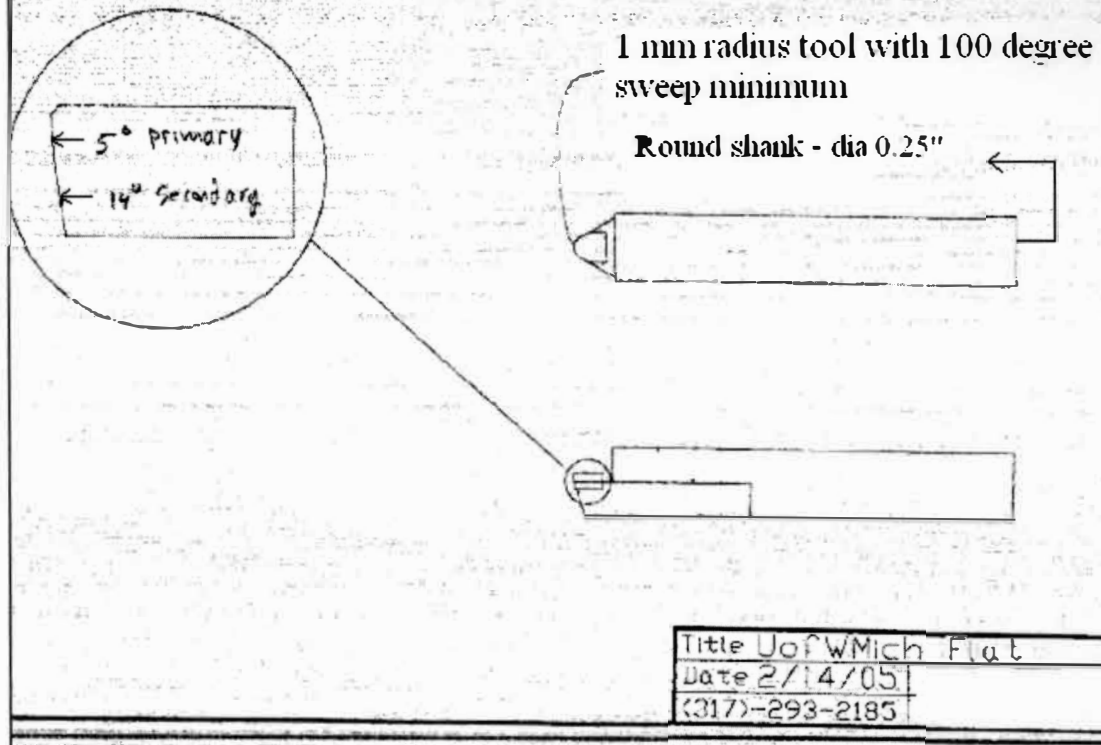


Figure F2: Design of a round nose diamond tool for SPDT of CVD coated SiC using the UMT